Weak Stability Boundary and Invariant Manifolds[*]

Edward Belbruno[†], Marian Gidea[‡], and Francesco Topputo[§]

Abstract. The concept of a weak stability boundary has been successfully used in the design of several fuel efficient space missions. In this paper we give a rigorous definition of the weak stability boundary in the context of the planar circular restricted three-body problem, and we provide a geometric argument for the fact that, for some energy range, the points in the weak stability boundary of the small primary are the points with zero radial velocity that lie on the stable manifolds of the Lyapunov orbits about the libration points L_1 and L_2, provided that these manifolds satisfy some topological conditions. The geometric method is based on the property of the invariant manifolds of Lyapunov orbits being separatrices of the energy manifold. We support our geometric argument with numerical experiments.

Key words. weak stability boundary, Lyapunov orbits, invariant manifolds

AMS subject classifications. 70F15, 70F07, 37D10

DOI. 10.1137/090780638

1. Introduction. The notion of a weak stability boundary (WSB) was first introduced heuristically by Belbruno in 1987 for designing fuel efficient space missions and was subsequently proven to be useful in related applications [2, 7, 5, 6, 12, 13, 3, 45, 33, 14, 35, 18, 4, 39, 38, 44]. The WSB can be used to construct low energy transfers to the Moon, requiring little or no fuel for capture into lunar orbit. The first application for an operational spacecraft occurred in 1991 with the rescue of the Japanese mission Hiten [7]. The WSB was also applied in the European Space Agency (ESA) spacecraft *SMART*-1 in 2004 (see [40]). The WSB technique will be applied again in ESA's mission BepiColombo to explore planet Mercury in 2013 (see [25]), and in some upcoming NASA missions.

A different methodology for designing fuel efficient trajectories, based on hyperbolic invariant manifolds, was proposed in [1, 26, 31, 32, 27, 28] and was successfully applied in several space missions (see also [21, 22, 23, 24]). In some of these works it has been suggested that the hyperbolic invariant manifold method can be used to explain the trajectories obtained through the WSB method. Supporting this assertion, García and Gómez present in [18] numerical explorations that suggests that, for some range of energies, the WSB is contained in the closure of the union of the stable manifolds of the periodic orbits about two of the equilibrium points of the planar circular restricted three-body problem.

[†]Department of Astrophysical Sciences, Princeton University, Peyton Hall, Ivy Lane, Princeton, NJ 08544 (belbruno@princeton.edu). This author's work was supported by NASA SMD/AISR grants NNG06GG55G and NNX09AK81G.

[‡]Department of Mathematics, Northeastern Illinois University, 5500 N. St. Louis Avenue, Chicago, IL 60625 (mgidea@neiu.edu). This author's work was partially supported by NSF grant DMS 0601016.

[§]Aerospace Engineering Department, Politecnico di Milano, Via La Masa 34, 20156 Milan, Italy (topputo@aero.polimi.it).

In this paper we use the separatrix property of the invariant manifolds of the periodic orbits about the equilibrium points to argue that, under some conditions, the points on the stable manifolds are WSB points. We support our geometrical argument with numerical experiments. Our result, corroborated by the result in [18], demonstrates, by double inclusion, that, for some range of energies, the WSB coincides with the set of points on the stable manifolds with zero radial velocity and negative Kepler energy relative to the small primary.

In section 2 we give some background on the planar circular restricted three-body problem. In section 3 we define the WSB as follows: in the context of the planar circular restricted three-body problem, for each radial segment emanating from the small primary, we consider trajectories that leave that segment at the periapsis of an osculating ellipse whose semimajor axis is a part of the radial segment; a trajectory is called n-stable if it makes n full turns around the small primary without going about the large primary and it has negative Kepler energy when it returns to the radial segment; otherwise the trajectory is called n-unstable; the points that make the transition from the n-stable regime to the n-unstable one are by definition the points of the WSB of index n. We make precise the meaning of a full turn about a primary through the measurement of the net change in the angle swept by the position vector. We also require that the n intersections of the trajectory with the radial line be transverse. In this way, the n-stability condition is an open condition, and the set of the n-stable points on the radial segment is a countable union of open intervals. Thus, the WSB consists of the union of endpoints of such intervals, resembling a Cantor set (in agreement with [18]). In section 4 we give a numerical and geometric argument for the fact that the points on the stable manifolds of the periodic orbits around the libration points L_1 and L_2, with the property that they have zero radial velocity and negative Kepler energy relative to the small primary, are contained in the WSB, for some range of energies. The key idea for our argument is the separatrix property of these invariant manifolds, meaning that these manifolds separate two types of motions: transfer orbits between the primaries, and nontransfer orbits. Section 5 exposes the main conclusions of this paper: *the WSB theory overlaps with the invariant manifold theory for a significant range of energies.*

It is important to note that the WSB is not an invariant object for the dynamics. It is therefore somewhat surprising that the WSB is related to hyperbolic invariant manifolds. The remarkable feature of the weak stability boundary is that the local behavior near the small primary and hence far from the equilibrium points is sufficient to assess whether the trajectory lies on the stable manifold of a periodic orbit near an equilibrium point.

We remark that the definition of the WSB does not rely on the existence of the hyperbolic invariant manifolds. That is, one can still define and apply the properties of the WSB in models where the hyperbolic invariant manifolds are no longer well defined or are not separatrices. Some examples include the elliptic restricted three-body problem and the bicircular restricted four body problem, for which WSB sets were computed in [38]. These problems are described by nonautonomous Hamiltonian systems where the notions of stable and unstable manifolds are not well defined in the phase space.[1] It seems possible that the WSB may turn out to

---

[1]One can transform a nonautonomous Hamiltonian system into an autonomous one by adding an extra variable symplectically conjugated with time. Then one can compute invariant manifolds for the extended system. However, these invariant manifolds contain a dependency on time, so they do not separate transfer orbits from nontransfer orbits. If one considers a time-discretization of the system by a Poincaré map, one obtains time-independent invariant manifolds, but these manifolds again do not separate transfer orbits from nontransfer orbits.

provide a good substitute for the hyperbolic invariant manifolds in such models (see [19]).

2. Background.

2.1. Planar circular restricted three-body problem.

The model that we use to describe the motion of an infinitesimal particle relative to the Earth-Moon system is the planar circular restricted three-body problem (PCRTBP). In this model, relative to an inertial frame, two primary bodies P_1, P_2 of masses $m_1 > m_2 > 0$, respectively, move under mutual gravity on circular orbits about their common center of mass. The third body P_3, assumed to be of infinitesimal mass, moves under the gravity of the primaries in the same plane. The motion of the primaries is not affected by the motion of the infinitesimal mass. In our case, P_3 represents a spacecraft, and P_1, P_2 represent the Earth and the Moon, respectively. Let the mass ratio of the small body to the total mass be $\mu = m_2/(m_1 + m_2)$. In the following we will consider $\mu = 0.0121506683$.

The motion of the infinitesimal mass, relative to a corotating coordinate system (x, y) with the origin at the center of mass of the two bodies, and in normalized units of distance, mass, and time, is described by the following equations (following [43]):

$$(2.1) \qquad \ddot{x} - 2\dot{y} = \frac{\partial \Omega}{\partial x}, \qquad \ddot{y} + 2\dot{x} = \frac{\partial \Omega}{\partial y},$$

where the effective potential Ω is given by

$$(2.2) \qquad \Omega(x, y) = \frac{1}{2}(x^2 + y^2) + \frac{1 - \mu}{r_1} + \frac{\mu}{r_2} + \frac{1}{2}\mu(1 - \mu),$$

with $r_1 = ((x + \mu)^2 + y^2)^{1/2}$, $r_2 = ((x + \mu - 1)^2 + y^2)^{1/2}$ as P_1, P_2 are located at $(-\mu, 0)$, $(1 - \mu, 0)$, respectively.

The problem has the symmetry

$$(2.3) \qquad (x, y, \dot{x}, \dot{y}, t) \longrightarrow (x, -y, -\dot{x}, \dot{y}, -t),$$

meaning that each solution of (2.1) either is symmetric or has a symmetric counterpart.

The motion described by (2.1) has five equilibrium points L_k, $k = 1, 2, \ldots, 5$, known as the Euler–Lagrange libration points. Three of these, L_1, L_2, and L_3, lie along the x-axis, at the approximate coordinates $x_1 = 0.8369147188$, $x_2 = 1.1556824834$, and $x_3 = -1.0050626802$, respectively. In our notation, L_1 lies between the Earth and Moon, and L_2 lies beyond the Moon. The other two points, L_4 and L_5, lie at the vertices of two equilateral triangles with common base extending from P_1 to P_2.

The system of differential equations (2.1) admits an integral of motion, the Jacobi integral,

$$(2.4) \qquad J(x, y, \dot{x}, \dot{y}) = 2\Omega(x, y) - (\dot{x}^2 + \dot{y}^2).$$

The projection of an energy manifold,

$$(2.5) \qquad \mathcal{J}(C) = \{(x, y, \dot{x}, \dot{y}) \in \mathbb{R}^4 | J(x, y, \dot{x}, \dot{y}) = C\},$$

onto the configuration space (x, y) is called a Hill region. The motion of P_3 is always confined to the Hill region of the corresponding Jacobi energy C. The boundary of a Hill region is a zero-velocity curve. The Hill regions vary with the Jacobi energy C (see [43]). The Jacobi constants corresponding to the libration points are $C_1 \approx 3.2003449098$, $C_2 \approx 3.1841641431$, $C_3 \approx 3.0241502628$, and $C_4 = C_5 = 3$.

2.2. Equations of motion in polar coordinates. The equations of motion (2.1) can be written in polar coordinates (r, θ) relative to P_2, where r is the distance from P_2 to P_3 and θ is the angle between the axis $P_1 P_2$ and $P_2 P_3$ measured counterclockwise. See [44].

If the motion of P_3 starts at the periapsis $(\dot{r} = 0)$ of an osculating ellipse around the Moon of semimajor axis a and eccentricity $e \in [0, 1)$, and has initial velocity v with respect to the sidereal reference frame, then we have

$$(2.6) \qquad r = a(1 - e), \qquad v = \sqrt{\frac{(1+e)\mu}{r}}.$$

The Jacobi integral of the motion takes the form $(\dot{r} = 0)$:

$$J(r, v, \theta) = (1 - \mu)\left[1 + 2r\cos\theta + \frac{2}{\sqrt{r^2 + 2r\cos\theta + 1}}\right] + \frac{2\mu}{r} + 2vr - v^2, \text{ or}$$

$$(2.7) \qquad J(r, e, \theta) = (1 - \mu)\left[1 + 2r\cos\theta + \frac{2}{\sqrt{r^2 + 2r\cos\theta + 1}}\right] + \frac{2\mu}{r}$$

$$+ 2\sqrt{\frac{(1+e)\mu}{r}}r - \frac{(1+e)\mu}{r}.$$

In the definition of the WSB, we will need to refer to the Kepler energy H_2 of P_3 with respect to the primary P_2. This is given by

$$(2.8) \qquad H_2 = \frac{1}{2}v^2 - \frac{\mu}{r}.$$

From (2.6) it follows that

$$(2.9) \qquad H_2 = \frac{(e - 1)\mu}{2r}.$$

2.3. Invariant manifolds of Lyapunov orbits. The collinear libration points L_i, $i \in \{1, 2, 3\}$, are of center-saddle type. For some range of energies C, there exists a one-parameter family of periodic orbits $\{\gamma_i(C)\}_C$, also called Lyapunov orbits, emanating from the libration point L_i. As the energy C is decreased, the Lyapunov family of L_i approaches the closest primary, and collision occurs. When the energy is further decreased, the Lyapunov family continues to periodic orbits around the closest primary; such orbits can describe multiple loops about the primary, which can eventually shrink or coalesce into one loop. See [43, 8, 16].

For fixed C in some appropriate energy range, each periodic orbit γ_i possesses stable and unstable manifolds $W^s(\gamma_i)$ and $W^u(\gamma_i)$. For some values of C, the manifolds experience collisions and close encounters with the primaries. To avoid ill-conditioning and increase of errors during numerical integration the equations of motion have been regularized, using Levi–Civita regularization [41, 43], when the motion of the small particle is inside a disc of radius 10^{-2} around either primary.

The stable and unstable manifolds are 2-dimensional manifolds locally diffeomorphic to cylinders in the 3-dimensional energy manifold, and they are separatrices of the dynamics restricted to the energy manifold (see [15]). This means that, for $C \lesssim C_2$, the trajectories starting inside the stable cylinder make a transfer from one lobe of the Hill region to the
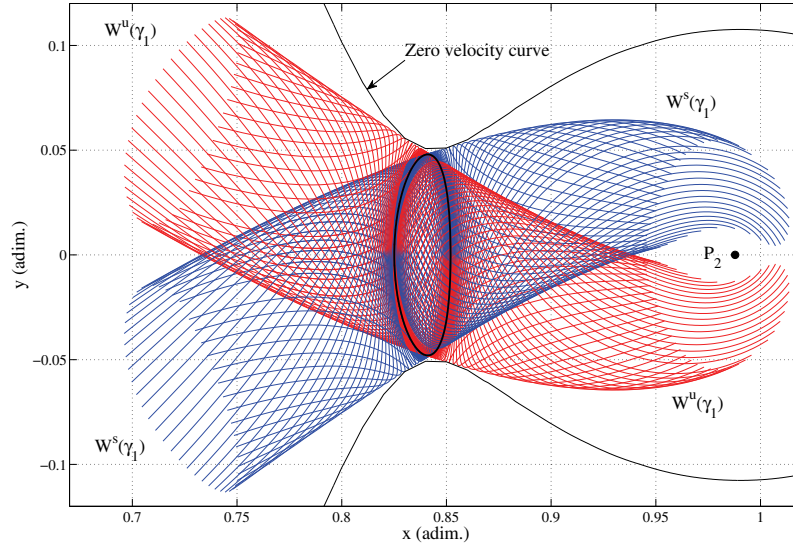
Figure 1. *Zero-velocity curves, Lyapunov orbit γ_1, and two branches of the stable and unstable manifolds, $W^s(\gamma_1)$ and $W^u(\gamma_1)$, for $C = 3.19$.*

other lobe or to the exterior region in forward time, while the trajectories starting inside the unstable cylinder make a transfer from one lobe of the Hill region to the other lobe or to the exterior region in backward time. See Figure 1.

2.4. Poincaré sections. We consider the cuts made by the stable and unstable manifolds of the Lyapunov orbits about L_1 and L_2 for a fixed Jacobi energy C, with a varying Poincaré section through P_2. Let

$$\mathcal{S}_{\theta_0} = \{(r, \dot{r}, \theta, \dot{\theta}) \,|\, \theta = \theta_0, \, \dot{\theta} > 0\}$$

be the Poincaré section through P_2 which makes an angle θ_0 with $P_1 P_2$. The coordinates $(r, \dot{r})$ of a point in $\mathcal{S}_{\theta_0}$ determines a unique trajectory through that point: the θ-coordinate equals θ_0 in this section, and the $\dot{\theta}$-coordinate can be solved uniquely from the energy condition $J(r, \dot{r}, \theta, \dot{\theta}) = C$, provided that $\dot{\theta} > 0$. Thus, each section $\mathcal{S}_{\theta_0}$ is plotted as an $(r, \dot{r})$-coordinate plane. The Poincaré first return map to $\mathcal{S}_{\theta_0}$ is denoted by Φ_{θ_0}.

We are interested in the successive cuts made by the invariant manifolds of γ_i, $i = 1, 2$, with $\mathcal{S}_{\theta_0}$, where γ_i is the Lyapunov orbit about L_i for a fixed energy level C. We label the cuts in such a way that the label of each cut matches with the number of complete turns about P_2 made by a trajectory starting from that cut until it approaches γ_i (in positive or negative time). We denote by $W^s_{\theta_0, j}(\gamma_i)$ the cut made by the stable manifold $W^s(\gamma_i)$ with $\mathcal{S}_{\theta_0}$ with the property that all the points in this cut make j complete turns about P_2 before approaching γ_i in forward time. Similarly, we denote by $W^u_{\theta_0, j}(\gamma_i)$ the cut made by the unstable manifold $W^u(\gamma_i)$ with $\mathcal{S}_{\theta_0}$ with the property that all the points in this cut make j complete turns about P_2 before approaching γ_i in backward time. These labels can be assigned inductively in the

manner described below.

Consider the branch of $W^s(\gamma_1)$ in the P_2-region and a varying Poincaré section $\mathcal{S}_{\theta_0}$ rotating clockwise about P_2. Assume that $W^s(\gamma_1)$ does not collide with P_2 and turns around P_2. Let $-\theta_1$ and θ_1 be the angles made by the tangent lines from P_2 to the Lyapunov orbit γ_1. For $-\theta_1 < \theta_0 < \theta_1$, the first cut between $W^s(\gamma_1)$ and $\mathcal{S}_{\theta_0}$ is not well defined, as the trajectories on the stable manifold approach γ_1 asymptotically and intersect $\mathcal{S}_{\theta_0}$ infinitely many times. If we rotate $\mathcal{S}_{\theta_0}$ clockwise to an angle $\theta_1 < \theta_0 < 2\pi - \theta_1$, the first cut between $W^s(\gamma_1)$ and $\mathcal{S}_{\theta_0}$ is well defined, but the trajectories starting from this first cut make less than 1 turn about P_2 before approaching γ_1. For these values of θ_0, we denote the first cut made by $W^s(\gamma_1)$ onto $\mathcal{S}_{\theta_0}$ by $W^s_{\theta_0,0}(\gamma_1)$. The angle $\theta(t)$ swept by a trajectory starting from $W^s_{\theta_0,0}(\gamma_1)$ until it approaches γ_1 asymptotically is less than 2π; that is, such a trajectory completes 0 turns about P_2. When we rotate $\mathcal{S}_{\theta_0}$ clockwise to an angle $2\pi - \theta_1 < \theta_0 < 2\pi + \theta_1$, the first cut of $W^s(\gamma_1)$ onto $\mathcal{S}_{\theta_0}$ is still well defined if we restrict the trajectories off some convenient neighborhood of γ_1. The angle $\theta(t)$ swept by a trajectory starting from this first cut until it approaches γ_1 asymptotically is a little more than 2π; thus such a trajectory completes 1 turn about P_2, and the cut is labeled by $W^s_{\theta_0,1}(\gamma_1)$. If we rotate clockwise $\mathcal{S}_{\theta_0}$ to an angle $2\pi + \theta_1 < \theta_0 < 4\pi - \theta_1$, the second cut of $W^s(\gamma_1)$ onto $\mathcal{S}_{\theta_0}$ consists of points that still make 1 turn about P_2 until they approach γ_1, so such a cut is denoted by $W^s_{\theta_0,1}(\gamma_1)$. For $4\pi - \theta_1 < \theta_0 < 6\pi - \theta_1$ a similar argument yields a cut with the property that the trajectories emerging from this cut complete 2 turns about P_2 until they approach γ_1, so such a cut is denoted by $W^s_{\theta_0,2}(\gamma_1)$. Inductively, this procedure produces a labeling $W^s_{\theta_0,j}(\gamma_1)$ for the cuts of $W^s(\gamma_1)$ onto $\mathcal{S}_{\theta_0}$ with $2j\pi - \theta_1 < \theta_0 < 2(j+1)\pi - \theta_1$, where $j \geq 0$. The trajectories starting from $W^s_{\theta_0,j}(\gamma_1)$ complete j turns about P_2 until they approach γ_1 in forward time. In a similar manner, one can produce a labeling $W^u_{\theta_0,j}(\gamma_1)$ of the cuts of $W^u(\gamma_1)$ with $\mathcal{S}_{\theta_0}$, such that the trajectories starting from $W^u_{\theta_0,j}(\gamma_1)$ make j turns about P_2 until they approach γ_1 in backward time. See Figure 2.

A similar procedure can be applied to label the cuts made by $W^s(\gamma_2)$ and $W^u(\gamma_2)$ with a varying Poincaré section $\mathcal{S}_{\theta_0}$ by $W^s_{\theta_0,j}(\gamma_2)$ and $W^u_{\theta_0,j}(\gamma_2)$, respectively, such that the label j equals the number of complete turns made by the infinitesimal mass about P_2 until it approaches γ_2 (in positive or negative time). The threshold values of the angle θ at which the number of complete turns about P_2 changes from $(j-1)$ to j are the values $2j\pi + \theta_2$, $j \geq 1$, where $-\theta_2$ and θ_2 represent the angles made by the tangent lines from P_2 to the Lyapunov orbit γ_2.

The successive cuts made by the invariant manifolds $W^{s,u}(\gamma_i)$ with the Poincaré sections are topological circles in $\mathcal{S}_{\theta_0}$ up to some number of turns about the primary. When the first transverse intersection of $W^u(\gamma_{i_1})$ and $W^s(\gamma_{i_2})$ occurs, where $i_1, i_2 \in \{1, 2\}$, some number of turns afterwards the topological circles are destroyed (see [20]). For example, if $W^s_{\theta_0,j}(\gamma_i)$ intersects transversally $W^u_{\theta_0,k}(\gamma_i)$ at some point P, then the kth negative iterate of $W^s_{\theta_0,j}(\gamma_i)$ under Φ_{θ_0}, which is $W^s_{\theta_0,j+k}(\gamma_i)$, is no longer a topological circle, but a finite union of curves open at both ends, whose ends wrap around $W^s_{\theta_0,j}(\gamma_i)$ infinitely many times. See Figure 3. Also, by Smale's homoclinic orbit theorem, the iterate $\Phi^{-k}_{\theta_0}$ of Φ_{θ_0} has a hyperbolic horseshoe near P; the orbits corresponding to the horseshoe display chaotic behavior that can be coded through symbolic dynamics. See [27, 20, 17, 36] as well as [10].
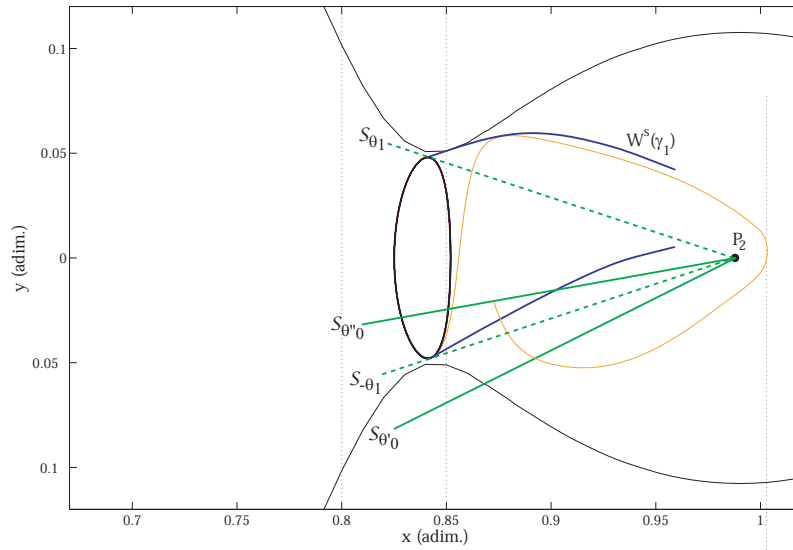
Figure 2. *A trajectory that completes* 0 *turns if it originates from* $\mathcal{S}_{\theta_0'}$ *with* $-\theta_1 < \theta_0' < 2\pi - \theta_1$, *and makes* 1 *complete turn around* P_2 *if it originates from* $\mathcal{S}_{\theta_0''}$ *with* $2\pi - \theta_1 < \theta_0'' < 4\pi - \theta_1$. *The angles are measured clockwise starting from* P_2P_1.
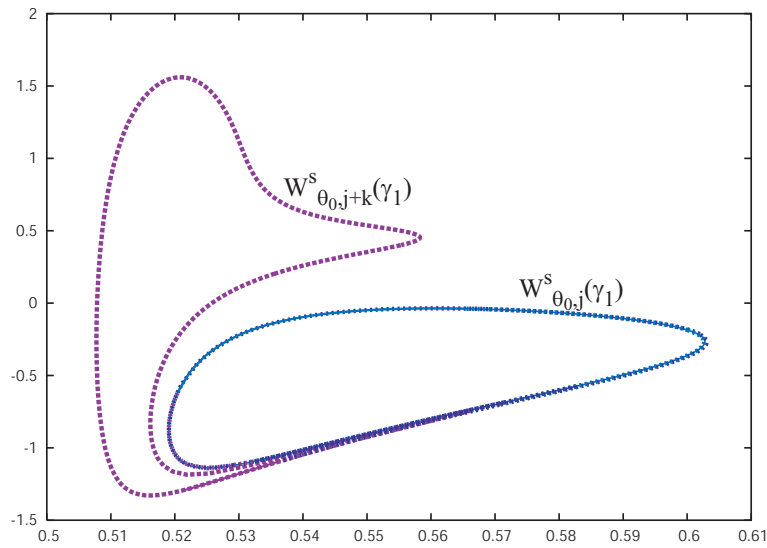

Figure 3. *Invariant manifold cut consisting of an open curve segment whose ends wrap some other invariant manifold cut.*

3. The WSB. In this section we give a rigorous algorithmic definition of the WSB (similar to that of [18]).

We consider trajectories of the infinitesimal particle with the following initial conditions:

(i) The initial position of the trajectory is on a radial segment $l(\theta)$ in the configuration space departing from P_2 and making an angle of θ with the P_1P_2 line, relative to the rotating system. The trajectory is assumed to start at the periapsis of an osculating ellipse around P_2, whose semimajor axis lies on $l(\theta)$ and whose eccentricity e is held fixed along $l(\theta)$. The initial velocity of the trajectory is perpendicular to $l(\theta)$; there are two different such choices of initial velocities, one positive (direct motion) and one negative (retrograde motion).

(ii) The initial Keplerian energy H_2 relative to P_2 is negative; i.e., $H_2 < 0$.

(iii) Then, the motion is said to be n-stable if the infinitesimal mass P_3 leaves $l(\theta)$ and makes n complete turns about P_2 *without* making a complete turn around P_1, and if the intersections of the trajectory with $l(\theta)$ along this trajectory are all transverse intersections and have negative Kepler energy with respect to P_2 (i.e., $H_2 < 0$). The motion is otherwise said to be n-unstable.

In condition (i) the distance from P_3 to P_2 is given by $r = a(1-e)$, where a is the semimajor axis of the osculating ellipse. The initial velocity vector fulfilling the above condition can be chosen in two ways, which differ from one another only by the sense of the vector. The initial radial velocity satisfies $\dot{r} = 0$. The motion, for fixed values of the parameters θ and e and for a choice of direction of the initial velocity vector, depends only on the initial distance r. Below, we will restrict ourselves to the case of positive initial velocity. The negative initial velocity case is discussed in [18, 38].

In condition (ii), the initial Kepler energy is given by (2.9), so the condition $H_2 < 0$ is automatically satisfied since $e \in [0, 1)$.

Since $v = r(1 + \dot{\theta})$, from (2.8) we obtain $H_2 = \frac{1}{2}r^2(1 + \dot{\theta})^2 - \frac{\mu}{r}$, so the condition $H_2 = 0$ defines a 2-dimensional surface in the 3-dimensional energy manifold $\{J = C\}$. This surface separates the energy manifold into two disjoint regions, where $H_2 < 0$ and $H_2 > 0$, respectively. Thus the condition that an intersection point of the trajectory with $l(\theta)$ has negative Kepler energy relative to P_2 means that the intersection point is in $\{J = C\} \cap \{H_2 < 0\}$.

In condition (iii), by P_3 making 1 complete turn around P_2 we mean the following. Let $\theta_2(t)$ be the angle made by the position vector of P_3 relative to P_2, measured continuously along the trajectory of P_3. If we consider that P_3 starts from $l(\theta)$, we have $\theta_2(0) = \theta$. Let τ_1 be the smallest positive time for which $\|\theta_2(\tau_1) - \theta_2(0)\| = 2\pi$. Assume that the intersection of the trajectory with $l(\theta)$ at $t = \tau_1$ is transverse (for a definition, see, e.g., [9]). If such a τ_1 exists, then we say that P_3 performed 1 complete turn around P_2 in the time interval $[0, \tau_1]$. Similarly, let τ_2 be the smallest positive time τ for which $\|\theta_2(\tau_2) - \theta_2(\tau_1)\| = 2\pi$. Assume that the intersection of the trajectory with $l(\theta)$ at $t = \tau_2$ is transverse. If such a τ_2 exists, then it means that P_3 performed 2 complete turns around P_2 in the time interval $[0, \tau_2]$. We can define inductively, in a similar fashion, what it means for P_3 to perform n complete turns about P_2. In this definition we require that the successive intersections of the trajectory of P_3 with $l(\theta)$ all be transverse.

In the same manner, we define what it means for P_3 to perform 1 complete turn about P_1. Also, if $\theta_1(t)$ is the angle made by the position vector of P_3 relative to P_1, measured continuously along the trajectory of P_3, if for some $\tau > 0$ we have $\|\theta_1(t) - \theta_1(0)\| < 2\pi$ for all $t \in [0, \tau]$, it means that P_3 did not perform 1 complete turn about P_1 in the interval $[0, \tau]$.

We note that in condition (iii) the initial point of the trajectory satisfies $\dot{r} = 0$, but the

subsequent intersections of the trajectory with $l(\theta)$ do not have to satisfy $\dot{r} = 0$. Also, between intersections, the Kepler energy H_2 is allowed to be locally positive. These two conditions are imposed only for applications to design low energy space missions and not for mathematical reasons.

In summary, condition (iii) says that a motion is said to be n-stable if there exist $\tau_n > 0$ such that P_3 performed n complete turns about P_2 in the interval $[0, \tau_n]$ and did not complete 1 turn around P_1 in the same interval.

In the above definition we require that the successive intersections of the trajectory of P_3 with $l(\theta)$ all be transverse. This generates the notion of n-stability under small perturbation; that is, if a trajectory is n-stable, then any sufficiently close trajectory will also be n-stable. This additional restriction does not have any practical consequences in the numerical computation of the WSB, as the initial conditions whose trajectories will fail the transversality condition have zero measure.

We note that the n-stability condition defined as above is an open condition. This is due to the fact that $H_2 < 0$ is an open condition, and that the mapping $\theta(0) \mapsto \theta(\tau_n)$ on $l(\theta)$ is smooth. The stability of the number of turns about a primary, as discussed earlier, implies that if for some value of r the motion is n-stable, then there exists a small $\delta > 0$ depending on r such that, for each $r' \in (r - \delta, r + \delta)$, the corresponding motion is also n-stable.

We have observed numerically that for any fixed value of the eccentricity $e \in [0, 1)$ all points $r \in l(\theta)$ that are sufficiently close to P_2 are n-stable. It seems possible that one can argue this behavior for sufficiently large positive values of the Jacobi energy and in some small open neighborhood of P_2 using the KAM theorem and the Nekhoroshev theorem (see [29, 37]).

Thus the set of the n-stable points on $l(\theta)$ is an open subset of $l(\theta)$; hence it is a countable union of open intervals, which we denote by

$$(3.1) \qquad \mathcal{W}_n(\theta, e) = \bigcup_{k \geq 1} (r_{2k-1}^*, r_{2k}^*)$$

with $r_1^* = 0$. The points r^* that are at the endpoints of intervals above (except for r_1^*) are n-unstable. In the numerical experiments, it would be impossible to detect a countable collection of stability intervals. The apparent Cantor-like structures of these sets, also noted in [18], support the possibility of having a countable collection of stability intervals. In this sense, our notion of stability seems to resemble KAM stability (see, e.g., [11]).

One example of unstable points is those lying on the stable manifold of the Lyapunov orbit, since they asymptotically approach the Lyapunov orbit and never return to $l(\theta)$.

By varying the parameters θ and e, we obtain the following stable sets:

$$\mathcal{W}_n(e) = \bigcup_{\theta \in [0, 2\pi]} \mathcal{W}_n(\theta, e),$$

$$\mathcal{W}_n = \bigcup_{\substack{\theta \in [0, 2\pi] \\ e \in [0, 1)}} \mathcal{W}_n(\theta, e).$$

These sets are also open sets since the n-stability of points depends smoothly on e and θ. We emphasize that it is essential in the definition of the WSB that the conditions (i)–(iii)

for n-stable points are open conditions to ensure the smooth dependence of the n-stability on e and θ.

We remark that $\mathcal{W}_m(e) \subset \mathcal{W}_n(e)$ and $\mathcal{W}_m \subset \mathcal{W}_n$ for $m > n$.

Definition 3.1. The WSB of index n, denoted by $\mathcal{W}_n^*$, is the locus of all points $r^*(\theta, e)$ along the radial segment $l(\theta)$ at which there is a change of stability of the initial trajectory; that is, $r^*(\theta, e)$ is one of the endpoints of an interval (r_{2k-1}^*, r_{2k}^*) characterized by the fact that for all $r \in (r_{2k-1}^*, r_{2k}^*)$ the motion is n-stable, and there exist $r', r'' \notin (r_{2k-1}^*, r_{2k}^*)$ arbitrarily close to r_{2k-1}^*, r_{2k}^*, respectively, for which the motion is n-unstable. Thus

$$\mathcal{W}_n^* = \partial \mathcal{W}_n = \{r^*(\theta, e) \,|\, \theta \in [0, 2\pi], e \in [0, 1)\}.$$

We also define

$$\mathcal{W}_n^*(e) = \partial \mathcal{W}_n(e) = \{r^*(\theta, e) \,|\, \theta \in [0, 2\pi]\}.$$

In Figure 4 we show the WSB sets $\mathcal{W}_n^*(e)$ for $n = 1$ and $e = 0.00$, $e = 0.20$, $e = 0.60$, and $e = 0.95$, which were generated by first computing the stable sets $\mathcal{W}_n(e)$ and then computing the boundary sets $\mathcal{W}_n^*(e) = \partial \mathcal{W}_n(e)$, using a bisection method as described in [44]. We emphasize that not all points in the same WSB set $\mathcal{W}_n^*(e)$ have the same Jacobi constant.

Remark 3.2. The WSB is not an invariant object for the dynamics. Moreover, the WSB is not a manifold but rather appears to be a fractal set. (Estimating the fractal dimension of the WSB is beyond the scope of this paper.) The WSB is concerned only with the behavior of a trajectory for some limited number of turns about the small primary. Counting the number of turns imposes some artificial cutoff conditions, in the sense that points with trajectories behaving rather similarly may be classified differently in terms of their stability, as they can differ in the number of turns about P_1 or P_2. For example, the trajectory in Figure 5(left) is 1-stable, although it seems that it completes 1 turn around P_1. In reality, the total angle swept by the trajectory relative to P_1 is a little less than 2π. On the other hand, the trajectory in Figure 5(right) is 1-unstable, although it is close to the previous orbit and is similar looking in the first part.

4. Weak stability boundary and invariant manifolds. In this section we describe a geometric mechanism that distinguishes n-stable points from n-unstable points and produces points in the WSB. This is based on the separatrix property of the hyperbolic invariant manifolds of the Lyapunov orbits. Then we present numerical experiments that verify the geometric mechanism.

4.1. Geometric mechanism. We give a geometric argument that, for some range of energies, the points on the stable manifold of the Lyapunov orbits about L_1 and L_2 belong to the WSB set, provided that they satisfy the zero radial velocity condition and the negative Kepler energy condition relative to the small primary. This argument is based on the fact that the invariant manifolds of the Lyapunov orbits are separatrices of the energy manifold in a neighborhood of the libration points. The stable and unstable manifolds of the Lyapunov orbits are global invariant objects diffeomorphic to 2-dimensional cylinders. The trajectories inside the cylinder bounded by the stable manifold of the Lyapunov orbit about L_1 or L_2 transfer from the P_2-region to the P_1-region or to the exterior region in forward time, while the trajectories outside the cylinder bounce back to the P_2-region and remain in that region
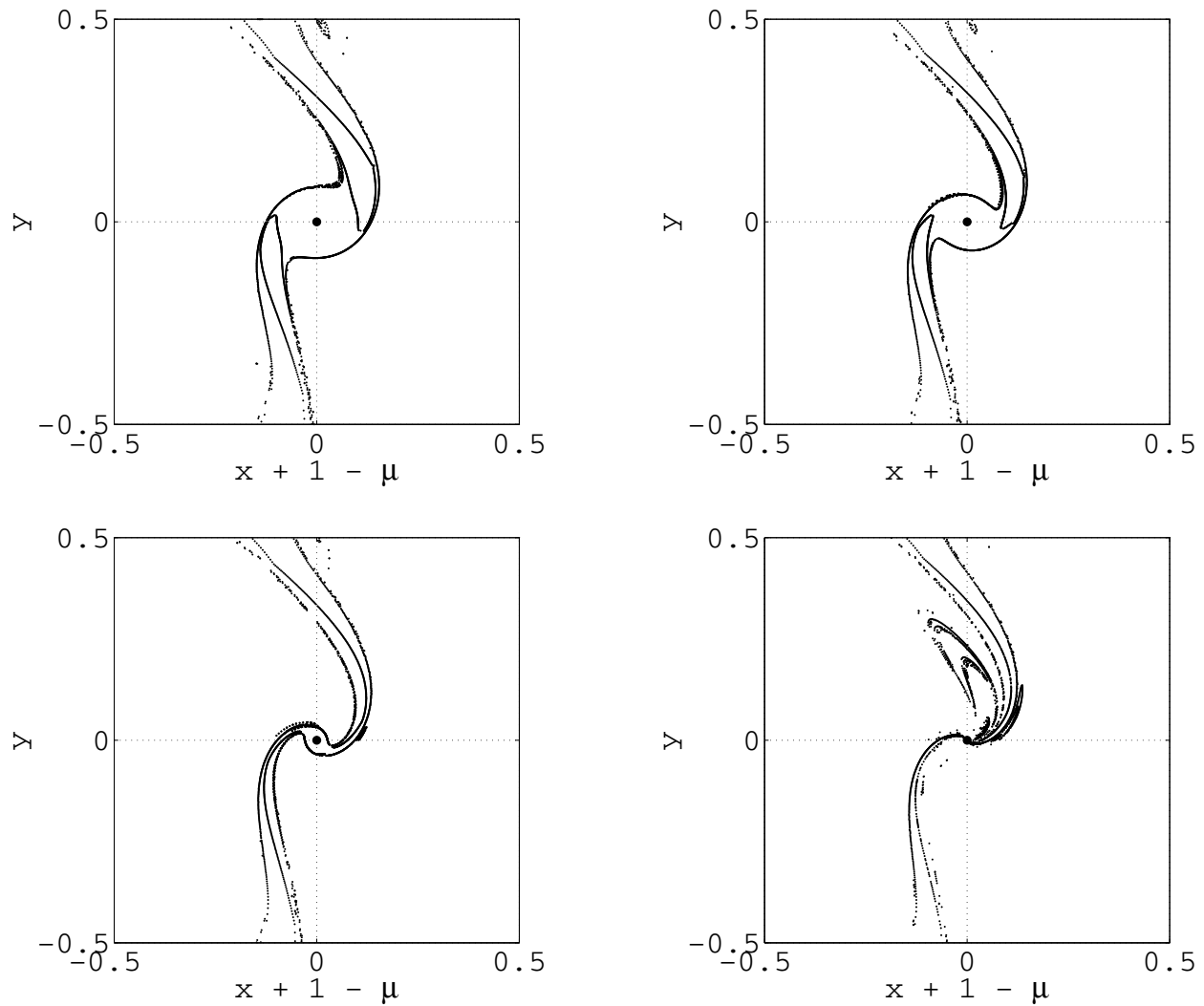
Figure 4. *Weak stability boundary sets $\mathcal{W}_1^*$ for eccentricities $e = 0.00$, $e = 0.20$, $e = 0.60$, $e = 0.95$.*

until they reach the interior of a cylinder. When these stable manifolds are cut by a plane of section that makes an angle of θ_0 with the axis between the primaries, the points in the section that are on the stable manifolds and that satisfy the zero radial velocity condition and the negative Kepler energy condition are points in the WSB: the nearby trajectories on one side of such points are stable orbits, while the nearby trajectories on the other side of such points are unstable orbits.

The geometric argument below relates the WSB set $\mathcal{W}_n^*$ with the stable manifolds of the Lyapunov orbits about L_1 and L_2. We assume the following topological conditions on the invariant manifolds of the Lyapunov orbits. These conditions are sufficient but not necessary.

Hypothesis A. We assume that the stable manifolds and unstable manifolds of the Lyapunov orbits γ_1 and γ_2 satisfy the following topological conditions:
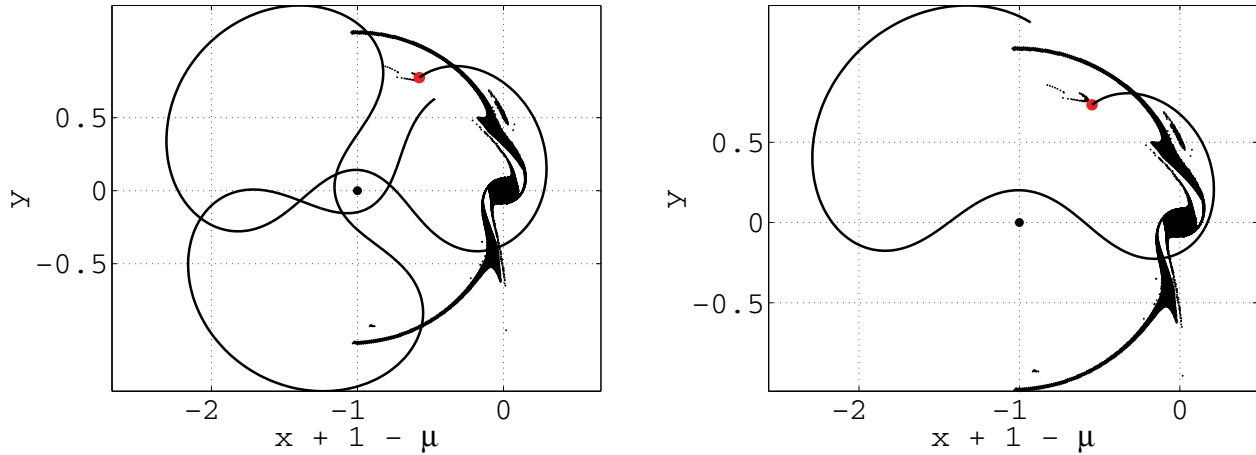
Figure 5. *A 1-stable trajectory that almost completes 1 turn about P_1 (left), and a 1-unstable trajectory that returns on $l(\theta)$ with positive Kepler energy (right). The initial condition is represented by the red point.*

(i) All the trajectories on the branch of $W^s(\gamma_1)$ in the P_2-region make at least n turns about P_2.

(ii) All the trajectories on the branch of $W^u(\gamma_1)$ in the P_1-region make at least 1 turn about P_1.

(iii) All the trajectories on the branch of $W^s(\gamma_2)$ in the P_2-region make at least n turns about P_2.

(iv) All the trajectories on the branch of $W^u(\gamma_2)$ in the exterior region make at least 1 turn about P_1.

For some values of μ and C there exist analytical arguments that ensure that some of these conditions are satisfied. In the case when the mass ratio μ is very small and (μ, C) is in some open set in the (μ, C) plane, the papers [34] and [30] imply conditions (i) and (iv) above. We do not know of analytical results to ensure conditions (ii) and (iii). In the case of the Sun-Jupiter system, for some values of $C < C_2$, numerical and analytical methods in [27] show the existence of a symbolic dynamics which ensures conditions (i)–(iv) for a certain range of values of n. A similar type of symbolic dynamics in the case of the Earth-Moon is more informally described in [28].

There are situations under which conditions (i)–(iv) above are not satisfied. For example, in the case when $W^u(\gamma_1)$ and $W^s(\gamma_1)$ collide with P_2 it is possible that these manifolds intersect at some point $x < 1 - \mu$, so there exist trajectories on $W^s(\gamma_1)$ that do not turn around P_2, so condition (i) fails. In a similar fashion, collisions of the other branches of the invariant manifolds with either P_1 or P_2 can yield trajectories that fail conditions (ii), (iii), or (iv). We will exclude these situations from the geometric analysis below.

We denote by $\mathcal{W}_n^{*,A}$ the subset of the WSB $\mathcal{W}_n^*$ for which the conditions of Hypothesis A are satisfied. We denote by $\mathcal{W}_n^{*,B}$ the complementary subset of $\mathcal{W}_n^{*,A}$ relative to $\mathcal{W}_n^*$.

In what follows, we will show that, for some range of energies $C > C_{\min}$,

$$(4.1) \qquad \mathcal{W}_n^{*,A} = \{(r, \dot{r}, \theta, \dot{\theta}) \in W_{\theta, n-1}^s(\gamma_1) \cup W_{\theta, n-1}^s(\gamma_2) \,|\, \dot{r} = 0, \, H_2 < 0\},$$
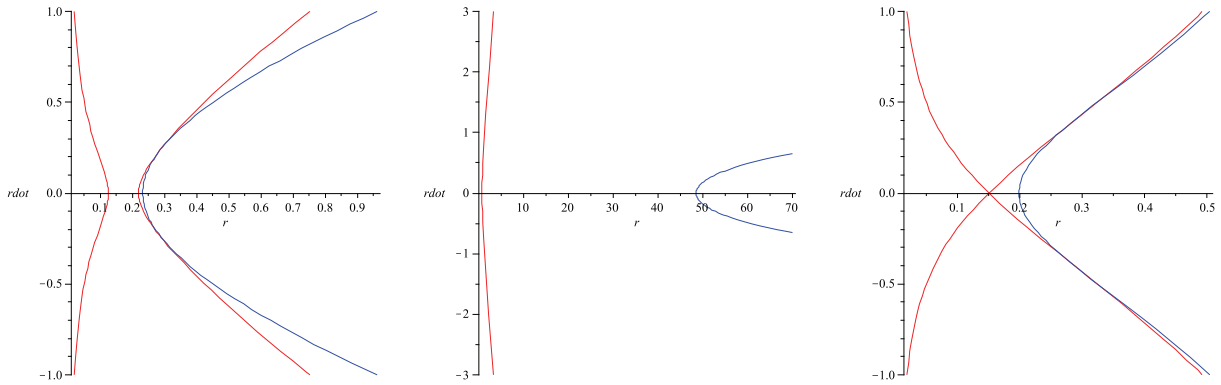
Figure 6. *The region $\{J = C_1\} \cap \{H_2 < 0\}$ in $(r, \dot{r})$-coordinates for θ fixed, where $\theta = 0$ (left), $\theta = \pm\pi/2$ (middle), and $\theta = -\pi$ (right). The red curves represent the boundary of $\{J = C_1\}$, and the blue curve represents $\{H_2 = 0\}$. In the left panel ($\theta = 0$) the red curve closest to the vertical axis corresponds to the boundary of the inner Hill region, while the farthest red curve corresponds to boundary of the outer Hill region. In the middle panel ($\theta = \pm\pi/2$) the blue curve is so distant from the vertical axis that the two red curves corresponding to the inner and outer boundaries of the Hill region cannot be distinguished in the plot. In the right panel ($\theta = -\pi$) the red curves correspond to boundaries of the two components of the inner Hill region. In each plot, the region between the vertical axis and the rightmost red curve represents $\{J = C_1\}$ and is always inside the region between the vertical axis and the blue curve, which represents $\{H_2 < 0\}$.*

where $W^s_{\theta,n-1}(\gamma_1)$ and $W^s_{\theta,n-1}(\gamma_2)$ represent the $(n-1)$th cut of $W^s(\gamma_1)$ and $W^s(\gamma_2)$ with the Poincaré section $\mathcal{S}_\theta$, where the cuts of the invariant manifolds are labeled as described in subsection 2.4.

4.1.1. Case $C \geq C_1$. When $C \geq C_1$ the Hill region is closed at L_1, so there are no transitions between the P_2-region and the P_1-region. Inside the P_2-region the condition $H_2 < 0$ is always satisfied; see Figure 6. Therefore all trajectories are n-stable for any n.

4.1.2. Case $C_2 < C < C_1$. We consider a Jacobi energy level $C_2 < C < C_1$. The corresponding Hill region is open at L_1 and closed at L_2, so transitions are possible between the P_2-region and the P_1-region but not between the inner and the outer region.

We consider the Lyapunov orbit γ_1 near the libration point L_1, corresponding to a fixed energy level, and the stable and unstable manifolds $W^s(\gamma_1)$ and $W^u(\gamma_1)$ of γ_1.

We relate the dynamics of points on the stable manifold $W^s(\gamma_1)$ to the dynamics of points in the WSB set $\mathcal{W}^{*,A}_n$. We label the successive cuts made by $W^s(\gamma_1)$ with $\mathcal{S}_{\theta_0}$ by $W^s_{\theta_0,j}(\gamma_1)$ in the manner as described in subsection 2.4, such that a trajectory starting from $W^s_{\theta_0,j}(\gamma_1)$ completes precisely j turns about P_2 before it approaches γ_1. By Hypothesis A(i), all the cuts with $0 \leq j \leq n$ are well defined.

It is possible that all successive cuts of the stable manifold with the section $\mathcal{S}_{\theta_0}$, up to the order $(n-1)$, are topological circles: $W^s_{\theta_0,0}(\gamma_1), W^s_{\theta_0,1}(\gamma_1), W^s_{\theta_0,2}(\gamma_1), \ldots, W^s_{\theta_0,n-1}(\gamma_1)$. If P is an initial point in $\mathcal{S}_{\theta_0}$ inside the region bounded by $W^s_{\theta_0,0}(\gamma_1)$, but sufficiently close to it, then the trajectory of P will make a transfer to the P_1-region by making less than 1 complete turn about P_2. If P is outside the region bounded by $W^s_{\theta_0,0}(\gamma_1)$ but sufficiently close to it, the trajectory will stay in the P_2-region for at least 1 turn. Similarly, if P is an initial point
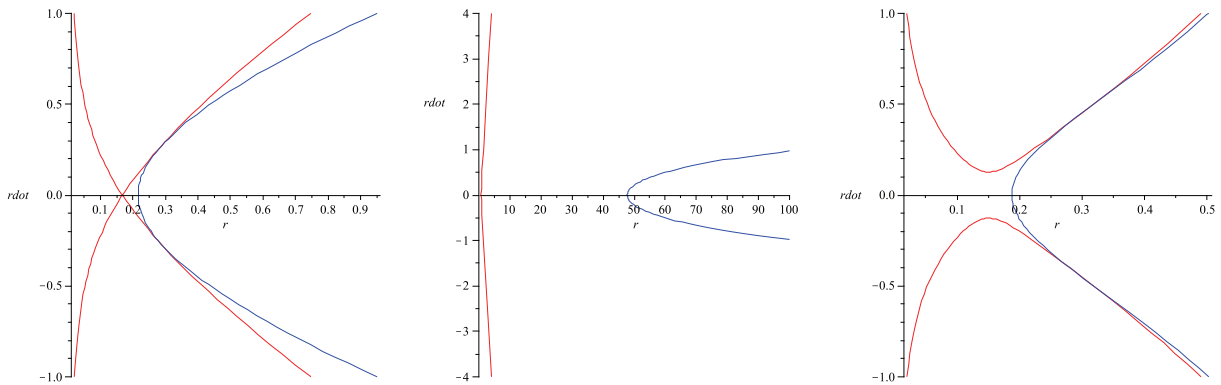
Figure 7. *The region $\{J = C_2\} \cap \{H_2 < 0\}$ in $(r, \dot{r})$-coordinates for θ fixed, where $\theta = 0$ (left), $\theta = \pm\pi/2$ (middle), and $\theta = -\pi$ (right). The red curve represents the boundary of $\{J = C_2\}$, and the blue curve represents $\{H_2 = 0\}$. The region between the vertical axis and the rightmost red curve represents $\{J = C_2\}$ and is always inside the region between the vertical axis and the blue curve, which is $\{H_2 < 0\}$.*

in $\mathcal{S}_{\theta_0}$ inside the region bounded by $W^s_{\theta_0,1}(\gamma_1)$, then the trajectory of P will make a transfer to the P_1 region by completing 1 turn about P_2 but turning less than 2 times about P_2. If P is outside the region bounded by $W^s_{\theta_0,1}(\gamma_1)$ but sufficiently close to it, the trajectory will stay in the P_2-region for at least 2 turns. In general, if P is an initial point in $\mathcal{S}_{\theta_0}$ inside the region bounded by $W^s_{\theta_0,n-1}(\gamma_1)$, then the trajectory of P will make a transfer to the P_1-region by completing $(n-1)$ turns about P_2 but turning less than n times about P_2, and if P is outside the region bounded by $W^s_{\theta_0,n-1}(\gamma_1)$ but sufficiently close to it, the trajectory will stay in the P_2-region for at least n turns. A trajectory that goes to the P_1-region enters it through the interior of the region bounded by unstable manifold $W^u(\gamma_1)$. By condition (ii) of Hypothesis A, the trajectory will make one or more complete turns around P_1 before it can return to the P_2-region. It is, of course, possible to also study trajectories that, once in the P_1-region, fail to make 1 complete turn around P_1 and then return to the P_2-region, but this will involve a more intricate analysis of the associated symbolic dynamics. We avoid this analysis here.

We represent the section $\mathcal{S}_{\theta_0}$ in coordinates $(r, \dot{r})$. In the case when the stable manifold cut $W^s_{\theta_0,n-1}(\gamma_1)$ transversally intersects the axis $\dot{r} = 0$ at some point w^* of coordinates $(r^*, 0)$, the points $(r, 0)$ with r near r^* will be interior points to $W^s_{\theta_0,n-1}(\gamma_1)$ on one side of $(r^*, 0)$ and exterior points to $W^s_{\theta_0,n-1}(\gamma_1)$ on the other side of $(r^*, 0)$. The exterior points $(r, 0)$ are n-stable, provided they satisfy the Kepler energy condition $H_2 < 0$. We note that not all points in this case satisfy the negative Kepler energy condition relative to P_2; see Figure 7. The interior points are n-unstable. The corresponding point w^* makes the transition from n-stability to n-instability, so it is a point in the WSB. Moreover, the eccentricity of the osculating ellipse at w^* can be computed from (2.6) as $e^* = \frac{(v^*)^2 r^*}{\mu} - 1$, where $v^* = r^*(1 + \dot{\theta}_{|\theta=\theta_0})$. Thus, the point w^* is in the WSB set $\mathcal{W}^{*,A}_n(\theta_0, e^*)$. If the cut $W^s_{\theta_0,n-1}(\gamma_1)$ does not intersect the axis $\dot{r} = 0$, it means that on the cut $W^s_{\theta_0,n-1}(\gamma_1)$ there are no WSB points from the set $\mathcal{W}^{*,A}_n(\theta_0, e)$ for any eccentricity e.

We remark that in the case when $\theta_0 = 0$ and $\theta_0 = \pi$ the WSB points in the section $\mathcal{S}_{\theta_0}$ are

symmetric homoclinic points. Indeed, the symmetry (2.3) implies that if $(r(t), \theta(t), \dot{r}(t), \dot{\theta}(t))$ is an orbit, then $(r(-t), -\theta(-t), -\dot{r}(-t), \dot{\theta}(-t))$ is also an orbit. Thus, an orbit that intersects $\mathcal{S}_{\theta_0}$ with $\dot{r} = 0$, for $\theta_0 = 0$ or $\theta_0 = \pi$, is a symmetric orbit. Since the stable and unstable manifolds are also symmetric, a point in $W^s_{\theta_0, n-1}(\gamma_1)$ with $\dot{r} = 0$ is a symmetric homoclinic point, provided $\theta_0 = 0$ or $\theta_0 = \pi$.

It is possible that not all the cuts made by the stable manifold with the plane of section are topological circles, as noted in subsection 2.4. If $W^s_{\theta_0, j}(\gamma_1)$ is a topological circle in $\mathcal{S}_{\theta_0}$ that intersects $W^u_{\theta_0, k}(\gamma_1)$, which is also a topological circle, then any intersection point is a homoclinic point that makes $j + k - 1$ turns around P_2, and the region bounded by both $W^s_{\theta_0, j}(\gamma_1)$ and $W^u_{\theta_0, k}(\gamma_1)$ consists of trajectories that make transitions to the P_1-region in negative time, after $j + k - 1$ turns about P_2. Thus $W^s_{\theta_0, j+k}(\gamma_1)$ is no longer a topological circle; it consists of a finite number of curves open at both ends that wrap asymptotically around $W^s_{\theta_0, j}(\gamma_1)$ infinitely many times. Although the topological circle property is lost, we can still distinguish between points "interior" to the region bounded by $W^s_{\theta_0, j+k}(\gamma_1)$ and "exterior" points (from the point of view of separatrix property): the interior points are precisely the image under $\Phi_{\theta_0}^{-k}$ of the points inside the region bounded by $W^s_{\theta_0, j}(\gamma_1)$ and outside the region bounded by $W^u_{\theta_0, k}(\gamma_1)$ in $\mathcal{S}_{\theta_0}$. The conclusion is that the points interior to the region bounded by $W^s_{\theta_0, j+k}(\gamma_1)$ correspond to trajectories that leave the P_2-region in $(j+k-1)$ turns, while the points exterior to the region bounded by $W^s_{\theta_0, j+k}(\gamma_1)$ correspond to trajectories that remain in the P_2-region for at least $(j + k)$ turns.

The same type of argument can be made when a broken topological circle, like $W^s_{\theta_0, j+k}(\gamma_1)$ above, intersects some unstable manifold cut $W^u_{\theta_0, \ell}(\gamma_1)$. All the points interior to the region bounded by both $W^s_{\theta_0, j+k}(\gamma_1)$ and $W^u_{\theta_0, \ell}(\gamma_1)$ correspond to trajectories that make a transition to the P_1-region in negative time, after $(j+k+\ell-1)$ turns about P_2. The return $W^s_{\theta_0, j+k+\ell}(\gamma_1)$ of $W^s_{\theta_0, j+k}(\gamma_1)$ to $\mathcal{S}_{\theta_0}$ under $\Phi_{\theta_0}^{-\ell}$ consists of a finite number of curves open at both ends that wrap asymptotically around the components of $W^s_{\theta_0, j+k}(\gamma_1)$ infinitely many times. The points interior to the region bounded by $W^s_{\theta_0, j+k+\ell}(\gamma_1)$ are the image under $\Phi_{\theta_0}^{-\ell}$ of the points interior to the region bounded by $W^s_{\theta_0, j+k}(\gamma_1)$ and exterior to $W^u_{\theta_0, \ell}(\gamma_1)$ in $\mathcal{S}_{\theta_0}$. The points interior to the region bounded by $W^s_{\theta_0, j+k+\ell}(\gamma_1)$ correspond to trajectories that leave the P_2-region in $(j + k + \ell - 1)$ turns, while the points exterior to the region bounded by $W^s_{\theta_0, j+k+\ell}(\gamma_1)$ correspond to trajectories that remain in the P_2-region for at least $(j + k + \ell)$ turns.

We conclude that the transverse intersection points between the stable manifold cut $W^s_{\theta_0, n-1}(\gamma_1)$ and the axis $\dot{r} = 0$ in $\mathcal{S}_{\theta_0}$ are points in the WSB set $\mathcal{W}^*_n(\theta_0, e^*)$ for some e^*, regardless of whether $W^s_{\theta_0, n-1}(\gamma_1)$ is a topological circle or not.

4.1.3. Case $C_{\min} < C < C_2$. We consider a Jacobi energy level $C_{\min} < C < C_2$ for some $C_{\min}$ large enough so that the Lyapunov orbits around L_1 and L_2 do not collide with P_2. A safe choice is $C_{\min} = 3.15$. The corresponding Hill region is open at both L_1 and L_2, so transitions are possible between the P_2-region and P_1-region and also between the inner region and the outer region. In the numerical computations in subsection 2.3 the value of $C_{\min}$ will be restricted by our numerical methods to compute the Lyapunov orbits and their invariant manifolds.

We consider the Lyapunov orbits γ_1 near the libration point L_1 and γ_2 near the libration point L_2, corresponding to a fixed energy level. We also consider the stable and unstable

manifolds $W^s(\gamma_1)$ and $W^u(\gamma_1)$ of γ_1, and the stable and unstable manifolds $W^s(\gamma_2)$ and $W^u(\gamma_2)$ of γ_2. The stable manifolds $W^s(\gamma_1)$ and $W^s(\gamma_2)$ never intersect, and the unstable manifolds $W^u(\gamma_1)$ and $W^u(\gamma_2)$ never intersect as well. On the other hand, the stable manifolds can pass very close to one another, and so can the unstable manifolds.

We label the successive cuts made by $W^s(\gamma_1)$ with the Poincaré section $\mathcal{S}_{\theta_0}$ by $W^s_{\theta_0,j}(\gamma_1)$ in the manner described in subsection 2.4, such that a trajectory starting from $W^s_{\theta_0,j}(\gamma_1)$ completes precisely j turns about P_2 before it approaches γ_1, and we denote the successive cuts made by $W^s(\gamma_2)$ with $\mathcal{S}_{\theta_0}$ by $W^s_{\theta_0,j}(\gamma_2)$, such that a trajectory starting from $W^s_{\theta_0,j}(\gamma_2)$ completes precisely j turns about P_2 before it approaches γ_2. By Hypothesis A(i) and (iii), all the cuts with $0 \leq j \leq n$ are well defined.

These successive cuts made by the stable manifolds with the surface of section are topological circles or broken circles, but in either case they bound regions with well-defined interior points (in the sense of the separatrix property), as explained in subsection 4.1.3. If an initial point P in $\mathcal{S}_{\theta_0}$ is a point interior to the region bounded by $W^s_{\theta_0,n-1}(\gamma_1)$, then the trajectory of P will complete $(n-1)$ turns about P_2 and make a transfer to the P_1-region. Once in the P_1-region, it will complete at least 1 turn about P_1 before it can return to the P_2-region, due to Hypothesis A(ii). On the other hand, if P is outside the region bounded by $W^s_{\theta_0,n-1}(\gamma_1)$ but sufficiently close to it, then the trajectory will stay in the P_2-region for at least n turns.

Similarly, if an initial point P in $\mathcal{S}_{\theta_0}$ is a point interior to the region bounded by $W^s_{\theta_0,n-1}(\gamma_2)$, then the trajectory of P will complete $(n-1)$ turns about P_2 and make a transfer to the exterior region. Once the trajectory is in the exterior region, it will complete at least 1 turn about P_1 before it can return to the interior region, according to Hypothesis A(iv). If P is outside the region bounded by $W^s_{\theta_0,n-1}(\gamma_2)$ but sufficiently close to it, the trajectory will stay in the P_2-region for at least n turns.

To detect the WSB points we consider the transverse intersection points w^* of the stable manifold cuts $W^s_{\theta_0,n-1}(\gamma_1) \cup W^s_{\theta_0,n-1}(\gamma_2)$ with the axis $\dot{r} = 0$ in $\mathcal{S}_{\theta_0}$. These intersection points are points in the WSB set $\mathcal{W}^*_n(\theta_0, e)$ for some e^*, provided that they satisfy the following conditions: (1) The points near w^* interior to $W^s_{\theta_0,n-1}(\gamma_1) \cup W^s_{\theta_0,n-1}(\gamma_2)$ satisfy the Kepler energy condition $H_2 < 0$. We note that not all points in this case satisfy the negative Kepler energy condition relative to P_2 (see Figure 8). (2) The points near w^* exterior to $W^s_{\theta_0,n-1}(\gamma_1) \cup W^s_{\theta_0,n-1}(\gamma_2)$ that leave the P_2-region make at least 1 full turn about P_1 inside the P_1-region or in the exterior region before they may eventually return to the P_2-region.

In addition, the points w^* as above that are found in a plane of section $\mathcal{S}_{\theta_0}$ with $\theta_0 = 0$ or $\theta_0 = \pi$ are symmetric homoclinic points.

Remark 4.1. The key geometrical argument in the above is that the stable and unstable manifolds of a Lyapunov orbit are 2-dimensional invariant manifolds that separate the 3-dimensional energy manifold. This shows that, for a fixed energy level, the corresponding WSB points lie on the stable manifold of the Lyapunov orbit. However, the WSB set consists of points on different energy manifolds. The WSB set itself is not an invariant manifold and does not have the separatrix property. As the WSB is not restricted to an energy manifold, the WSB concept can be extended to other situations where energy manifolds are not invariant or where stable invariant manifolds of periodic orbits cannot be defined.

Remark 4.2. In the case when $W^s_{\theta_0,n-1}(\gamma_i)$ is a broken topological circle consisting of infinitely many open curves that wrap asymptotically about some $W^s_{\theta_0,m}(\gamma_1)$ with $m < n-1$,
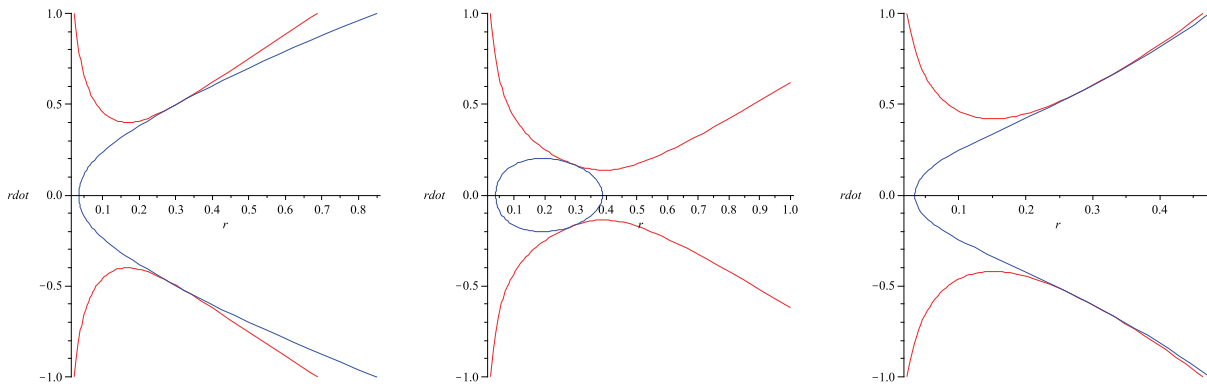
Figure 8. *The region $\{J = C_3\} \cap \{H_2 < 0\}$ in $(r, \dot{r})$-coordinates for θ fixed, where $\theta = 0$ (left), $\theta = \pm\pi/2$ (middle), and $\theta = -\pi$ (right). The red curve represents the boundary of $\{J = C_3\}$, and the blue curve represents $\{H_2 = 0\}$. The region between the vertical axis and the rightmost red curve represents $\{J = C_3\}$ and is always inside the region between the vertical axis and the blue curve, which is $\{H_2 < 0\}$.*

each intersection point w_j^* between such a component and the axis $\dot{r} = 0$ in $\mathcal{S}_{\theta_0}$ yields a point in the WSB set $\mathcal{W}_n^*(\theta_0, e_j^*)$ for some e_j^*. We emphasize here that the eccentricities of the osculating orbits corresponding to the points w_j^* are all different, although very close to one another, so these points belong to different WSB sets $\mathcal{W}_n^{*,A}(e)$ of different eccentricities e, such as those in Figure 4. However, a small change in the energy level of γ_i yields a small change in the positions w_j^* and hence of the corresponding eccentricities e_j^* of the osculating ellipses. Thus, through a sequence of successive small perturbations of the energy level we can slightly move each point w_j^*, one at a time, so that all resulting points will have the same eccentricity for their osculating ellipses (with the resulting points w_j^* at different energy levels). Here we recall that the WSB sets $\mathcal{W}_n^{*,A}(e)$ contain points not necessarily at the same energy level. This perturbation argument supports the possibility of having a countably infinite collection of stable intervals (r_{2k-1}^*, r_{2k}^*) in (3.1), and could perhaps explain some of the fine Cantor set–like structures that are visible in some regions of the WSB sets. See the plots in Figure 4.

Remark 4.3. It seems possible to analyze the WSB in the context of the planar Hill problem. The structure of invariant manifolds of periodic orbits near the equilibrium points is similar to that in the PCRTBP [42]. It is expected that the same relationship between the WSB and the stable invariant manifold of periodic orbits holds in the planar Hill problem as in the PCRTBP.

4.2. Numerical experiments. We describe a numerical algorithm to test that the points on the WSB coincide with the points on the stable manifolds of the Lyapunov orbits which satisfy the zero radial velocity condition and the negative Kepler energy condition relative to the small primary. This algorithm is centered on the idea that the hyperbolic invariant manifolds are separatrices of the energy manifold. We illustrate this algorithm with several examples and discuss the results.

In subsection 4.1 we provided a geometric argument to show that, for some range of energies,

(4.2) $\{(r, \dot{r}, \theta, \dot{\theta}) \in W_{\theta,n-1}^s(\gamma_1) \cup W_{\theta,n-1}^s(\gamma_2) \,|\, \dot{r} = 0,\, H_2 < 0\}$

is the subset $\mathcal{W}_n^{*,A}$ of $\mathcal{W}_n^*$, consisting of the WSB points for which the invariant manifolds of the Lyapunov orbits by L_1 and L_2 satisfy some topological conditions described by Hypothesis A. However, Hypothesis A is a sufficient condition for a point in $\mathcal{W}_n^*$ to be in the set (4.2), but not necessary. It is possible that the stable and unstable manifolds of γ_1 and γ_2 as a whole fail Hypothesis A, but nevertheless individual trajectories on those manifolds exhibit behavior consistent with the conditions of Hypothesis A. The numerical experiments below detect the points in $\mathcal{W}_n^*$ that are also in the set (4.2); we will call these points of type A. There are also points in $\mathcal{W}_n^*$ that are not in the set (4.2); we will call these points of type B. The set of all points of type A includes $\mathcal{W}_n^{*,A}$.

In what follows, we will numerically compute $\mathcal{W}_n^*$ and identify the subset of points of type A as the WSB points that satisfy (4.2) modulo some margin of error. The numerical algorithm consists of the following steps:

(1) We numerically compute the WSB set $\mathcal{W}_n^*(e)$ for a fixed number of turns n and for a fixed eccentricity e. We limit our analysis to points with energy $C_{\min} < C < C_2$. This computation is done in two steps. In the first step we compute the n-stable set $\mathcal{W}_n(e)$. For this, we divide the eccentricity range into a grid of values $e = \{0, 0.05, \ldots, 0.95\}$. We fix one value of e at a time and compute the corresponding n-stable orbits as follows. We choose a range of radius values around P_2 and approximate this range by a grid of values $r \in \{0, 2 \cdot 10^{-3}, \ldots, 1.5\}$. We also approximate the angular range $\theta \in [0, 2\pi]$ around P_2 by a grid of values $\theta \in \{0, 2\pi \cdot 10^{-3}, \ldots, 2\pi\}$. For each fixed θ from the grid, we consider an initial point (r, θ) with r from the grid, and an initial velocity perpendicular to the position vector (r, θ), of size v given by (2.6). We integrate this initial condition forward in time in polar coordinates with respect to both P_2 and P_1. The evolution in time of the angle swept around P_2 and P_1 is tracked, and the negative Kepler energy relative to P_2 is verified at the intersection points with $l(\theta)$. The point is redeemed as n-stable or n-unstable according to the algorithmic definition in section 3. The coordinates $(r, \dot{r}, \theta, \dot{\theta})$ and the Jacobi constant C of each n-stable point are recorded. The Jacobi constant is also given by (2.7). In the second step, the WSB is computed as the boundary set $\mathcal{W}_n^*(e) = \partial(W_n(e))$ of the n-stable set, using a bisection algorithm. The output is a data set of points w_i^* with their coordinates and Jacobi constants. The details of this computation are given in [44].

(2) For each fixed value of the eccentricity e, the points w_i^* of the WSB set $\mathcal{W}_n^*(e)$ are analyzed one at a time with respect to their relationship to the stable manifolds of the Lyapunov orbits. Each point is retrieved from the data set together with its coordinates $(r_i^*, \dot{r}_i^*, \theta_i^*, \dot{\theta}_i^*)$ and the corresponding Jacobi constant C_i.

(3) For each Jacobi constant C_i the Lyapunov orbits γ_1 and γ_2 are computed numerically.

(4) The stable manifolds $W^s(\gamma_1)$ and $W^s(\gamma_2)$ are integrated numerically in polar coordinates relative to P_2.

(5) The stable manifolds $W^s(\gamma_1)$ and $W^s(\gamma_2)$ are cut with the Poincaré section $\mathcal{S}_{\theta_i^*}$, where θ_i^* is the angle coordinate associated with the point r_i^*. The Poincaré section $\mathcal{S}_{\theta_i^*}$ is represented in the coordinates $(r, \dot{r})$. The points in the $(n-1)$th cut of $W^s(\gamma_1)$ and $W^s(\gamma_2)$ with the Poincaré section are retained.

(6) The intersection points between $W^s(\gamma_1) \cup W^s(\gamma_2)$ and the axis $\dot{r} = 0$ in $\mathcal{S}_{\theta_i^*}$ are computed numerically. As, in general, there might be several such intersection points,

only one of them, $w_i^{**} = (r_i^{**}, 0, \theta_i^{**}, \dot{\theta}_i^{**})$, will have the eccentricity of the corresponding osculating ellipse equal to e, modulo some small margin of error. Moreover, we select only those points w_i^{**} that have negative Kepler energy relative to P_2

(7) We select the points w_i^* that are within a small margin of error from the corresponding points w_i^{**}. These are the points of type A, and they include the set $\mathcal{W}_n^{*,A}$, the set of points in $\mathcal{W}_n^*$ that satisfy Hypothesis A. The complementary set is the points of type B. The practical method for selecting the points of type A is the following. We compute the Euclidean distance in phase space between the original point w_i^*, computed through the bisection algorithm, and the new point w_i^{**}, computed as the cuts between the stable manifold and the axis $\dot{r} = 0$ in the the Poincaré section:

$$d = \|w_i^* - w_i^{**}\|.$$

We select only those points w_i^{**} for which the distance from the corresponding w_i^* is within a tolerance of $\delta = 10^{-3}$. (Since our numerical procedures are automatic procedures that explore a large number of points in the WSB sets, generate the Lyapunov orbits for the energy level of each point on the WSB, integrate the stable manifolds of these Lyapunov orbits, compute and count the cuts of these manifolds with Poincaré sections of prescribed angles, and detect the intersection of these cuts with $\dot{r} = 0$, we found that this indirect procedure to identify the subset $\mathcal{W}_n^{*,A}$ is computationally effective. It is nevertheless true that these procedures have intrinsic limitations by the choice of algorithm for each component numerical routine, and by numerical errors.)

(8) To the selected points w_i^{**}, found in the intersections between the stable manifold and the axis $\dot{r} = 0$ in the Poincaré section, we apply a test to verify numerically that they make the transition between n-stability and n-instability. This test confirms that the selected points w_i^{**} are in the WSB set $\mathcal{W}_n^*(e)$. For a given point $w_i^{**} = (r_i^{**}, 0, \theta_i^{**}, \dot{\theta}_i^{**})$, two nearby points w_i' and w_i'' are chosen on the radial line $\theta = \theta_i$, of coordinates $w_i' = (r_i', \dot{r}_i', \theta_i', \dot{\theta}_i')$ and $w_i'' = (r_i'', \dot{r}_i'', \theta_i'', \dot{\theta}_i'')$. The coordinates are chosen so that w_i' and w_i'' are in the same Poincaré section $\mathcal{S}_{\theta_i^*}$ as w_i^{**} and their associated osculating ellipses have the same eccentricity e as w_i^{**}, i.e., $r_i' = r_i^{**} + \epsilon$, $\dot{r}_i' = 0$, $\theta_i' = \theta_i^*$, $\dot{\theta}_i' = \sqrt{\frac{\mu(1+e)}{(r_i')^3}} - 1$, and $r_i'' = r_i^{**} - \epsilon$, $\dot{r}_i'' = 0$, $\theta_i'' = \theta_i^*$, $\dot{\theta}_i'' = \sqrt{\frac{\mu(1+e)}{(r_i'')^3}} - 1$, where $\epsilon = 10^{-8}$. The points w_i' and w_i'' are integrated forward in time in polar coordinates with respect to both P_2 and P_1. The evolution in time of the angle swept around P_2 and P_1 is tracked, and the negative Kepler energy condition relative to P_2 is verified at the intersection points with $l(\theta_i^*)$. This test is assessed as successful if one of the points w_i', w_i'' is redeemed as n-stable and the other one is redeemed as n-unstable. In the numerical examples explored, all selected points are found to satisfy this condition.

Example 4.4. An example of applying the algorithm is illustrated in Figure 9. We select a point w_i^* from the WSB set $\mathcal{W}_1^*(0)$ in a Poincaré section $\mathcal{S}_{\theta_i^*}$, $\theta_i^* \simeq 3\pi/4$. The Lyapunov orbits γ_1 and γ_2 for the Jacobi constant $C_i = 3.1645669491$ corresponding to the point w_i are computed numerically. The stable manifold $W^s(\gamma_1)$ is cut with the Poincaré section $\mathcal{S}_{\theta_i^*}$. This cut is $W_{\theta_i^*,0}^s(\gamma_1)$, as the points in the cut complete 0 turns about P_2 before approaching γ_1. The intersection between $W^s(\gamma_1)$ and the axis $\dot{r} = 0$ in $\mathcal{S}_{\theta_i^*}$ is identified. In the same plot, the original point w_i^* is shown. The intersection w_i^{**} between $W_{\theta_i^*,0}^s(\gamma_1)$ and the axis $\dot{r} = 0$ in
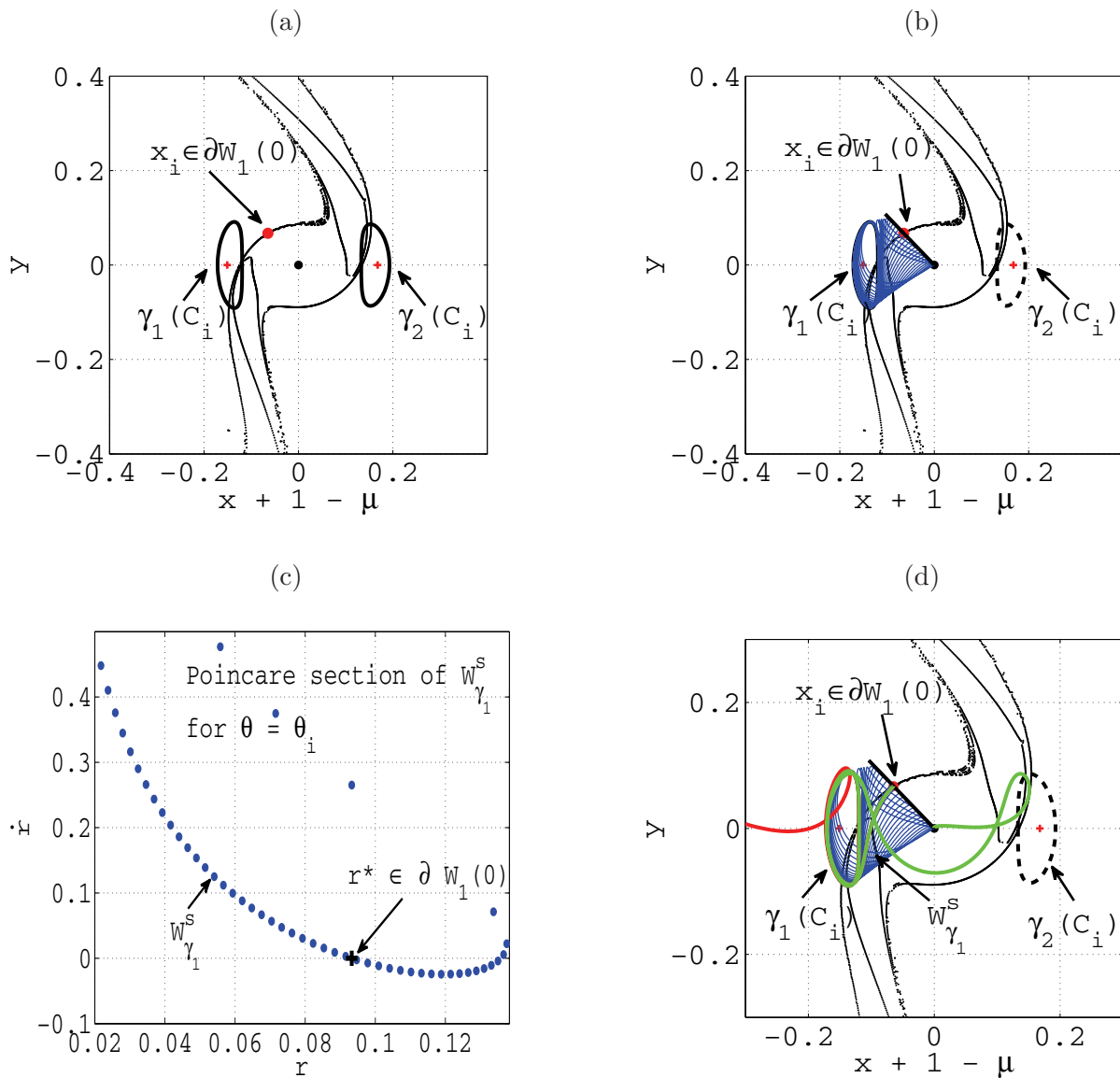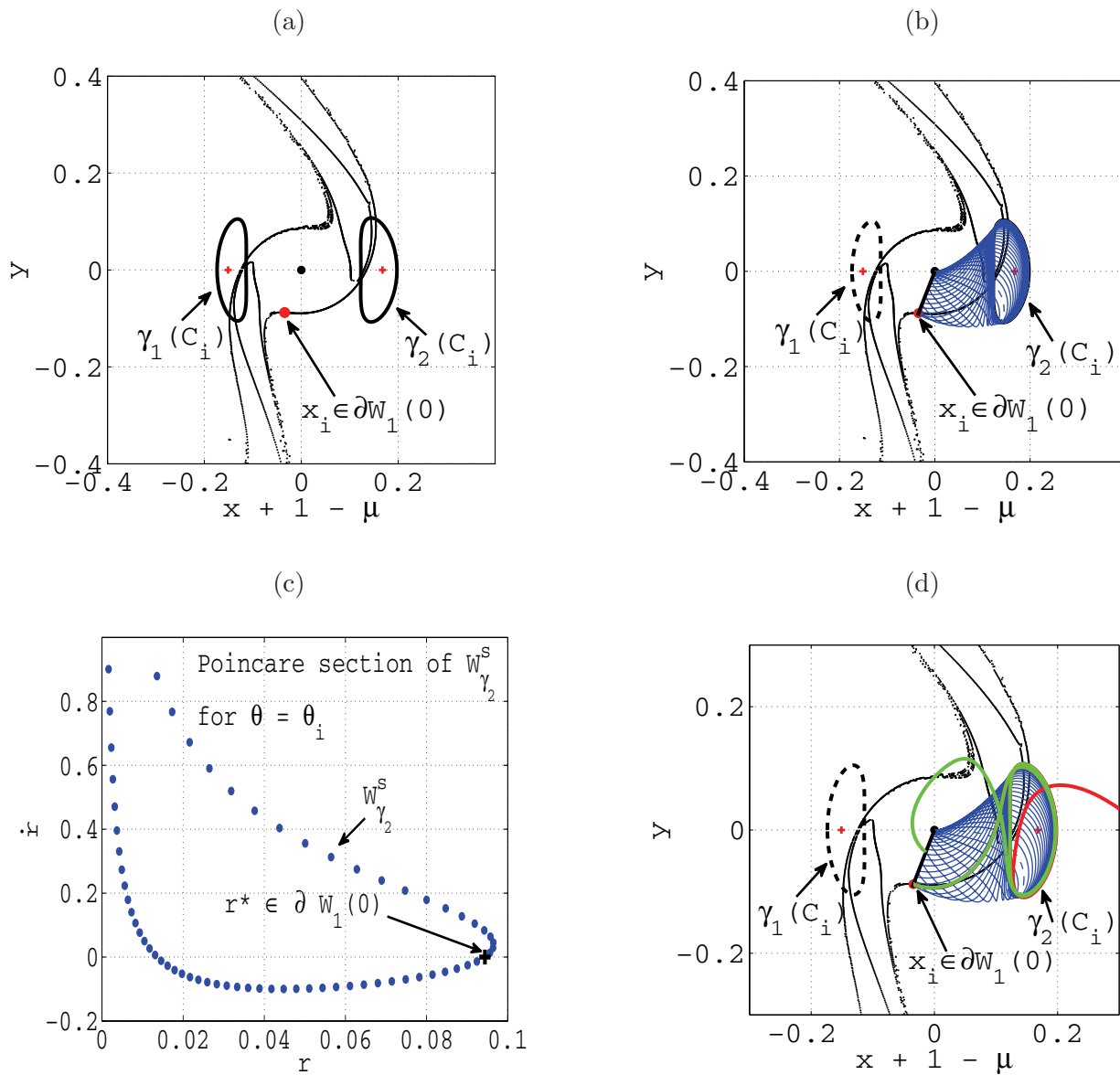
Figure 9. (a) *A point in the WSB and the Lyapunov orbits for the corresponding energy level.* (b) *The stable manifold of the Lyapunov orbit about L_1.* (c) *The cut made by the stable manifold with the Poincaré section and its intersection with $\dot{r} = 0$.* (d) *Forward integration of two initial points near the intersection of the stable manifold with $\dot{r} = 0$.*

$\mathcal{S}_{\theta_i^*}$ and the original point w_i^* almost overlap in the plot. The points w_i^* and w_i^{**} are within a δ-tolerance, so the point $w_i^* \approx w_i^{**}$ is of type A. To apply the test described in step (8) of our algorithm, the intersection point between $W^s(\gamma_1)$ and the axis $\dot{r} = 0$ is fixed, and two nearby points in $\mathcal{S}_{\theta_i^*}$, with the eccentricities of the associated osculating ellipses chosen to be $e = 0$, are chosen. The two nearby points are integrated forward in time. The trajectories of the two points show that one is 1-stable and the other one is 1-unstable, which confirms our test.

Figure 10. (a) *A point in the WSB and the Lyapunov orbits for the corresponding energy level.* (b) *The stable manifold of the Lyapunov orbit about L_2.* (c) *The cut made by the stable manifold with the Poincaré section and its intersection with $\dot{r} = 0$.* (d) *Forward integration of two initial points near the intersection of the stable manifold with $\dot{r} = 0$.*

Example 4.5. Another example of applying this algorithm is illustrated in Figure 10. This is similar to the previous example, with the only difference being that the WSB point selected matches a point on the stable manifold $W^s(\gamma_2)$ of the Lyapunov orbit about L_2 for the Jacobi constant $C_i = 3.1539757951$.

Example 4.6. We restrict our analysis to an energy range $C \in [C_{\min}, C_2]$, and we consider the WSB sets $\mathcal{W}_n^*(e)$ with $n = 1, 2$ and $e = 0.4$. We match the points w_i^* obtained from
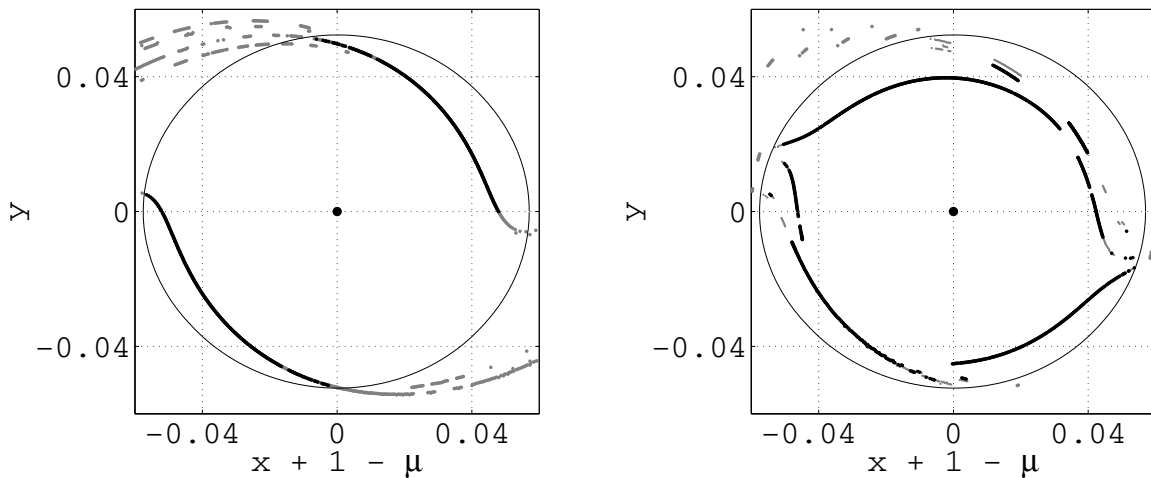
Figure 11. *Set of points on the WSB selected according to the criteria described in step* (7) *of our algorithm. The black points are points w_i^{**} that are within δ from the corresponding points w_i^*; these are type A points. Left: $n = 1$ and $e = 0.4$. Right: $n = 2$ and $e = 0.4$.*

the algorithmic definition of the WSB as in step (1) with the points w_i^{**} obtained from the $(n-1)$th cut of $W^s(\gamma_1)$ or $W^s(\gamma_2)$ with Poincaré section $\mathcal{S}^{\theta_i^*}$ intersected with the axis $\dot{r} = 0$ inside this section, as described in step (6).

In Figure 11 the displayed curve represents the points (r, θ) for which $J = C_{\min}$ for e fixed (see (2.7)). The gray points are the points w_i^* found by the algorithmic definition as in step (1). The points w_i^* in the interior region bounded by the curve are those that satisfy the energy restriction $C \in [C_{\min}, C_2]$. The points displayed in black are the points w_i^{**} that are obtained as in step (7). These are the points of type A, and they contain $\mathcal{W}_n^{*,A}$. Thus, for these points we have a matching between the WSB points obtained through the algorithmic definition and the points obtained through the invariant manifold approach.

There are a few WSB points in the interior region bounded by the energy condition curve which do not match with points on the stable manifolds. These are the points of type B. These are points whose trajectories experience close encounters or symbolic dynamics. In Figure 12 a type A point and a type B point of the WSB are chosen inside the region bounded by the energy curve. The trajectory of the type A point asymptotically approaches a Lyapunov orbit for the corresponding energy level; therefore the type A point lies on the stable manifold of the Lyapunov orbit. Meanwhile the trajectory of the type B point undergoes a close encounter with the primary.

In Figure 13 we show the trajectories of a collection of type A points chosen from the WSB. These trajectories asymptotically approach the Lyapunov orbit about L_1 or the Lyapunov orbit about L_2 corresponding to the energy level. Therefore these points lie on the union of the stable manifolds of the Lyapunov orbits about L_1 and L_2.

In Figure 14 we show the distribution of errors $d = \|w_i^* - w_i^{**}\|$ for the type A points, for $C = [C_{min}, C_2]$, $n = 1, 2$, and $e = 0.4$. The horizontal axis represents the angle coordinate θ about P_2, while the vertical axis shows the distance between the original point w_i^* from $\mathcal{W}_n^*(e)$
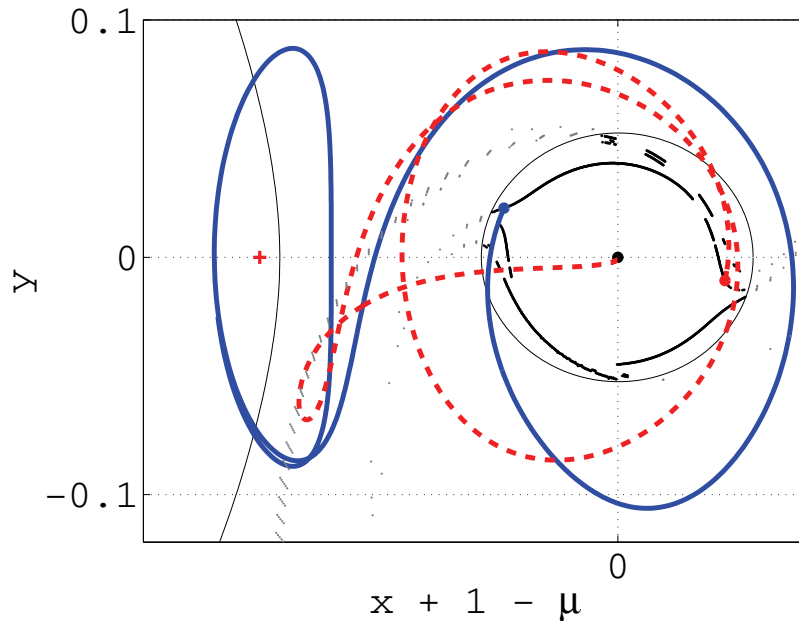
Figure 12. *Trajectory of a type A point lying on the stable manifold of a Lyapunov orbit (solid). Trajectory of a type B point undergoing a close encounter with the primary (dashed).*

and the matching point at the corresponding intersection between $W^s(\gamma_1)$ or $W^s(\gamma_2)$ and the axis $\dot{r} = 0$ in $\mathcal{S}_{\theta_i^*}$. Most of these selected points meet a tolerance level of 10^{-4}, while a few of them meet only a tolerance level of 10^{-3}.

Example 4.7. In the WSB there are regions where the points of $W^s(\gamma_1)$ are intertwined with those of $W^s(\gamma_2)$; see Figure 15. Since the points in $W^s(\gamma_1)$ and $W^s(\gamma_2)$ cannot overlap, we want to examine this region more closely. For example, we choose a point $w_i^* \in \mathcal{W}_1^*(0)$ of Jacobi constant $C_i = 3.159347461$. We compute the stable manifolds $W^s(\gamma_1)$ and $W^s(\gamma_2)$, and we intersect them with the corresponding Poincaré section $\mathcal{S}_{\theta_i^*}$. In this section, the cut made by $W^s(\gamma_2)$ appears to be a topological circle, and the cut made by $W^s(\gamma_1)$ appears to be a broken circle. Both circles intersect the horizontal axis $\dot{r} = 0$. Zooming in, although both intersections are close to the original point w_i^* on the WSB, it turns out that it is the intersection point w_i^1 of $W^s(\gamma_1)$ with $\dot{r} = 0$ that is closer; see Figure 16. Of course, $W^s(\gamma_2)$ also has an intersection point w_i^2 with $\dot{r} = 0$ in the section, but this point does not correspond to $e = 0$, so it actually belongs to a different WSB set $\mathcal{W}_1^*(e)$ with $e \neq 0$ small. When we take both intersection points w_i^1, w_i^2 and integrate them forward, the point w_i^1, which is essentially the same as the original point on the WSB, when flown forward, generates an orbit that gets close to γ_2 (because this point is close to $W_{\gamma_2}^s$), but then it changes course and asymptotically approaches γ_1 (because it is on $W_{\gamma_1}^s$); see Figure 15. This orbit is close to a heteroclinic connection between γ_2 and γ_1. For comparison, we also integrate forward the second point w_i^2, which is also close to the original point w_i^* on the WSB. This second orbit is asymptotic to γ_2. The orbits of w_i^1 and of w_i^2 are very close to one another and seem to overlap for a while, but their final behavior is rather different. Note that the plotted orbits do not remain
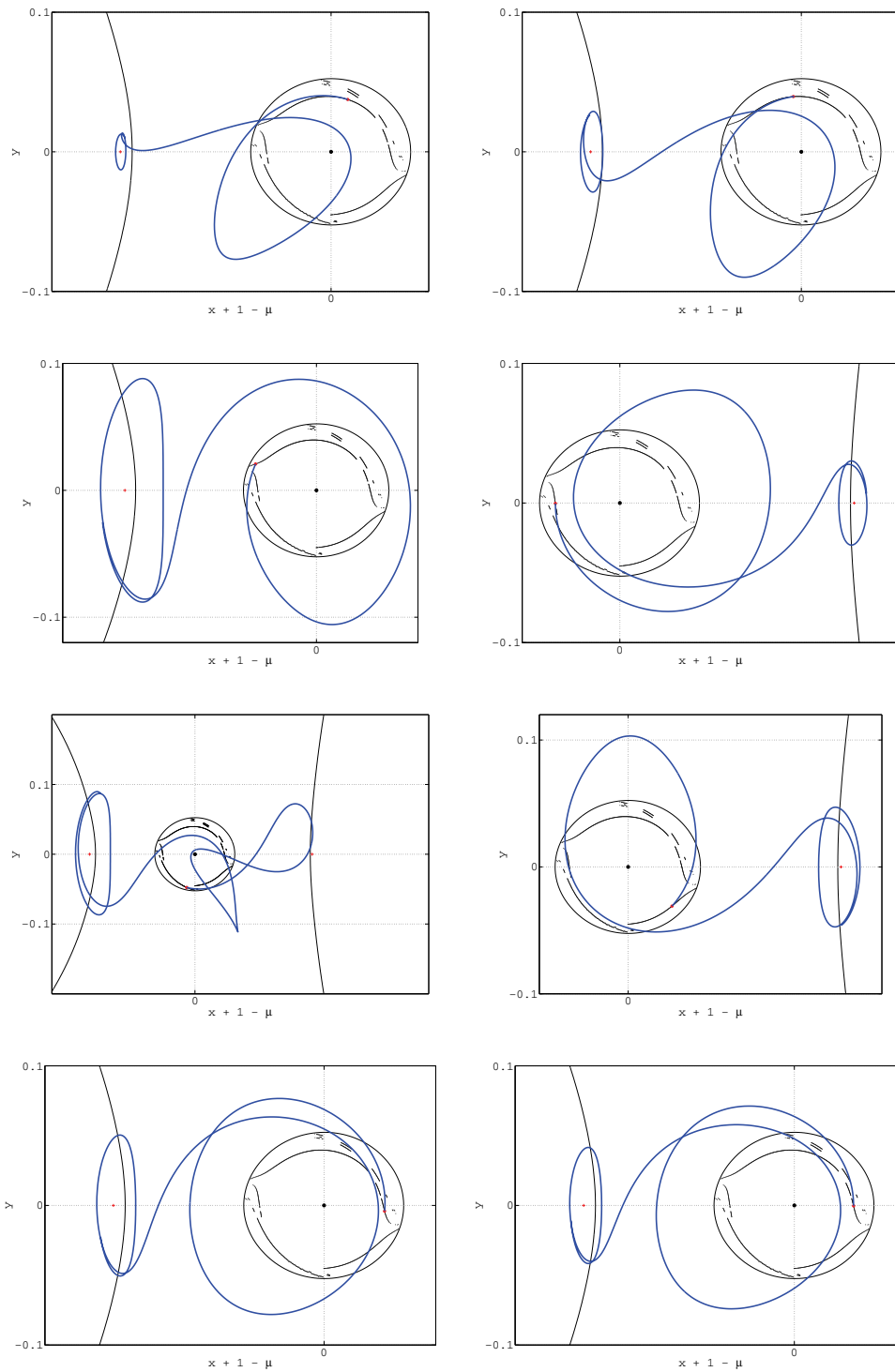
Figure 13. *Collection of trajectories of type A points lying on the stable manifolds of Lyapunov orbits for the corresponding energies.*
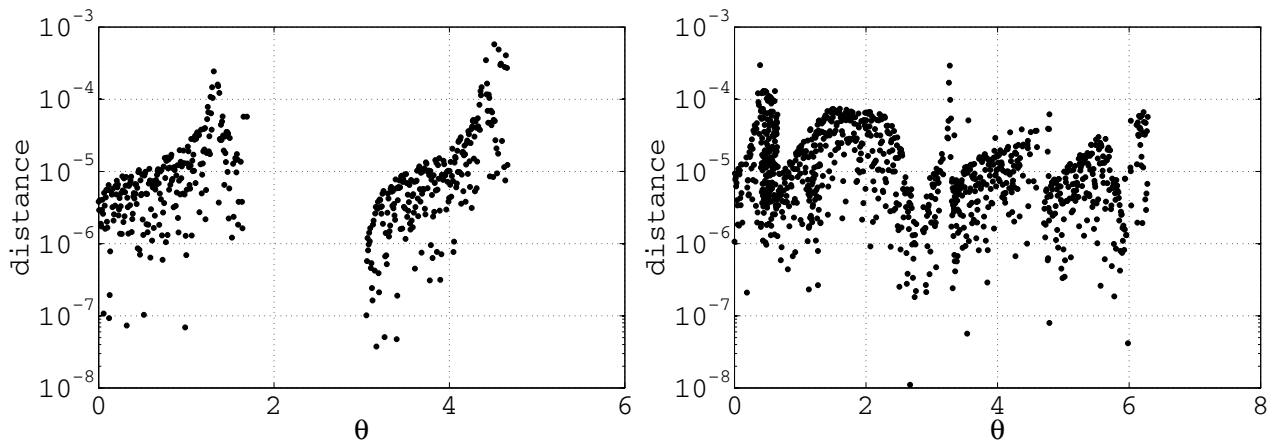
Figure 14. *Distribution of errors between the weak stability points and the points on the stable manifolds that satisfy the zero radial velocity condition and the negative Kepler energy condition relative to P_2. The horizontal axis represents the angle coordinate θ about P_2, and the vertical axis represents the distance between the points. Left: $n = 1$ and $e = 0.4$. Right: $n = 2$ and $e = 0.4$.*
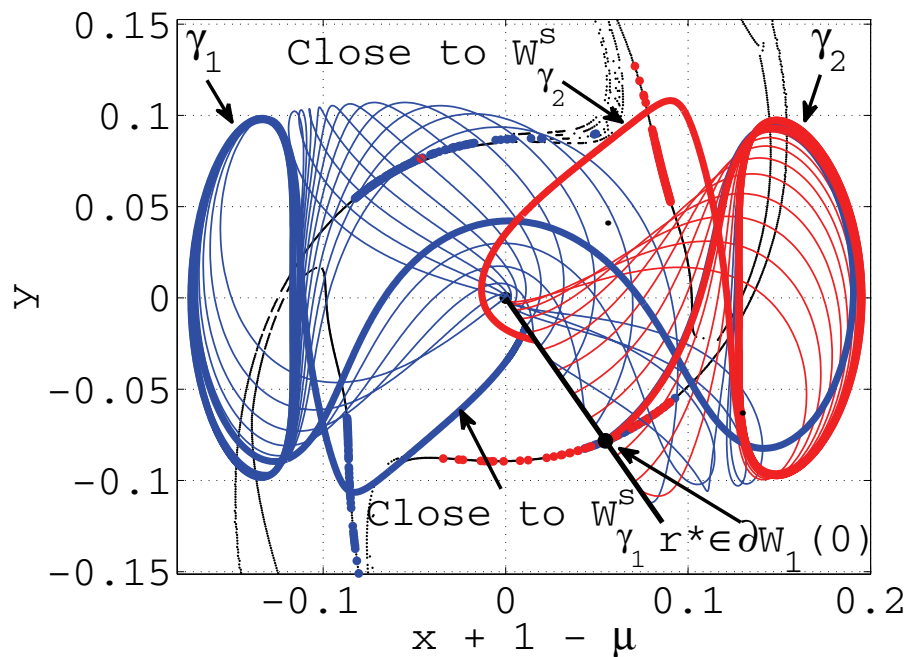

Figure 15. *The blue points in the WSB correspond to $W^s(\gamma_1)$, and the red points correspond to $W^s(\gamma_2)$. Forward integration of two initial points in the intersections of $W^s(\gamma_1)$ and $W^s(\gamma_2)$ with $\dot{r} = 0$.*

close to γ_1 and γ_2, respectively, as theoretically predicted, due to the numerical manifolds computed.

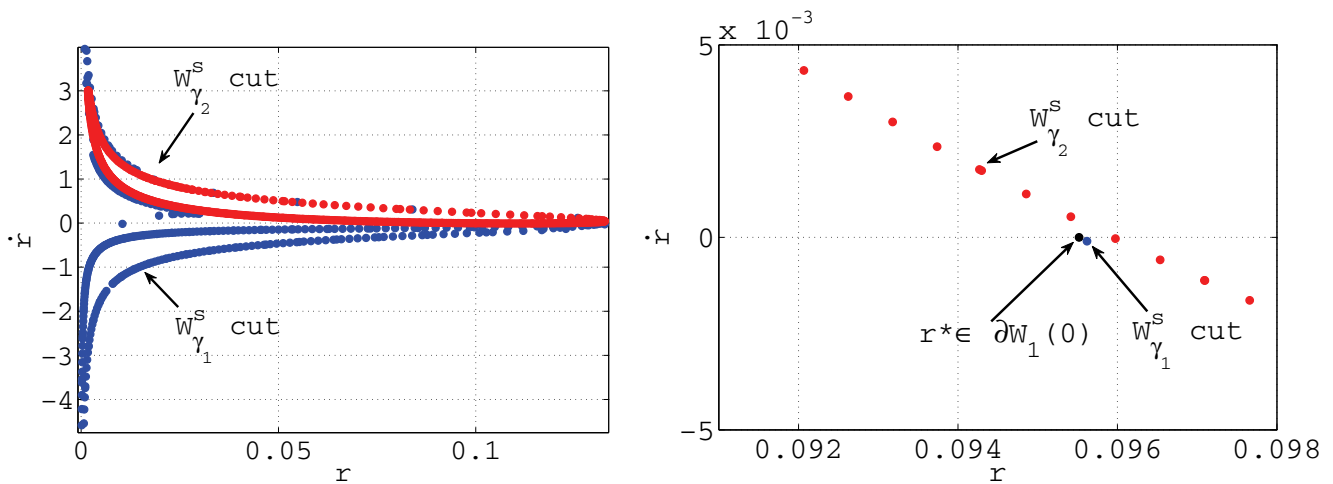*Example* 4.8. An important remark is that the points in the WSB set $\mathcal{W}_n^*(e)$ in general

Figure 16. *Left: the cuts made by $W^s(\gamma_1)$ and $W^s(\gamma_2)$ to a Poincaré section. Right: identification of a point in the WSB.*
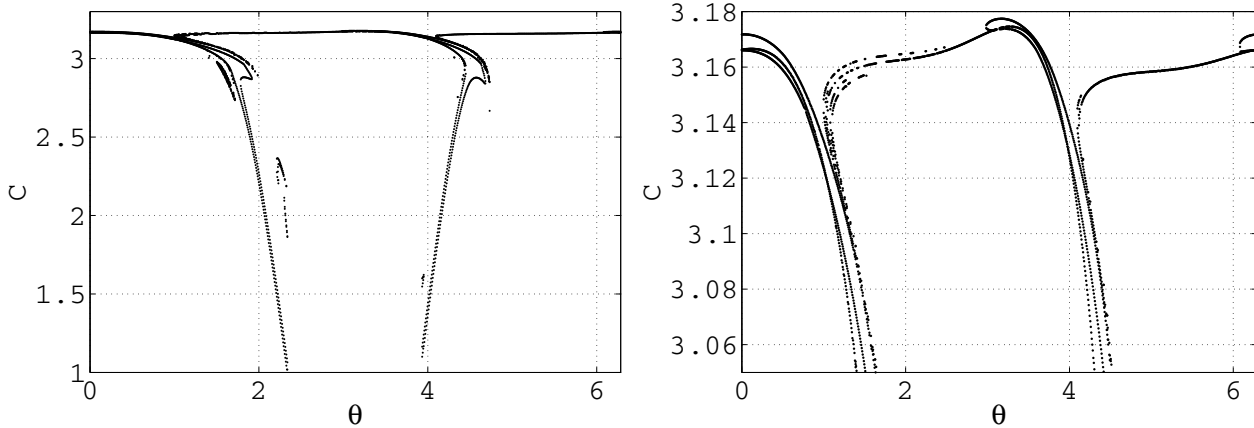

Figure 17. *The distribution of Jacobi constants corresponding to $\mathcal{W}_1^*(0)$ plotted against the angle θ about P_2.*

lie on different Jacobi energy levels. Indeed, for a fixed value of the eccentricity e and a fixed radial axis $l(\theta)$, a point $w^* \in \mathcal{W}_n^*(e)$ corresponds to a precise Jacobi energy level $J(r^*, \theta, e)$ given by (2.7). Thus, by moving along the radial axis $l(\theta)$, J changes according to (2.7). However, only certain points on the radial axis $l(\theta)$ will be in the WSB set $\mathcal{W}_n^*(e)$. When the Jacobi constant corresponding to $\mathcal{W}_1^*(0)$ is plotted versus the angle θ, one obtains the structure shown in Figure 17. The two dips in the plot correspond to the two spiral arms of the set $\mathcal{W}_1^*(0)$. We note that the points on the two spiral arms reach very low values of the Jacobi energy, corresponding to the case when the Hill region allows a trajectory to move within the entire plane.

4.3. Summary of geometrical and numerical arguments. We provided a geometrical argument that for a range of energy $C \in [C_{\min}, C_1]$, $C_{\min} = 3.15$, the points on $W^s(\gamma_1) \cup W^s(\gamma_2)$

that have zero radial velocity and negative Kepler energy relative to P_2 are part of the WSB set, provided that the invariant manifolds of γ_1 and γ_2 satisfy some topological conditions described in Hypothesis A. The geometrical argument relies on the separatrix property of the invariant manifolds. We considered the cuts $W^s_{\theta_0,n-1}(\gamma_1)$ and $W^s_{\theta_0,n-1}(\gamma_2)$ made by $W^s(\gamma_1)$ and $W^s(\gamma_2)$ with $\mathcal{S}_{\theta_0}$. If a point is outside the region bounded by $W^s_{\theta_0,n-1}(\gamma_1)$ or $W^s_{\theta_0,n-1}(\gamma_2)$, then it will stay in the P_2-region for at least n turns around P_2. If a point is inside the region bounded by $W^s_{\theta_0,n-1}(\gamma_1)$ or $W^s_{\theta_0,n-1}(\gamma_2)$, then it will leave the P_2-region after $(n-1)$ turns around P_2, and then it will make a complete turn around P_1. Thus the points on $W^s_{\theta_0,n-1}(\gamma_1)$ and $W^s_{\theta_0,n-1}(\gamma_2)$ with $\dot{r} = 0$ and $H_2 < 0$ are points in $\mathcal{W}^*_n$.

We numerically verified this geometric argument for a selection of points. We computed the WSB set for a fixed eccentricity e. For a given point in the WSB we computed $W^s(\gamma_1)$ and $W^s(\gamma_2)$, and their cuts $W^s_{\theta_0,n-1}(\gamma_1)$ and $W^s_{\theta_0,n-1}(\gamma_2)$ with $\mathcal{S}_{\theta_0}$. We intersected the cuts with $\dot{r} = 0$ and with the $H_2 < 0$ set. We found that one of these intersection points coincides, within some tolerance, with the original point chosen from the WSB. We tested the point by taking two nearby initial conditions inside the plane of section $\theta = \theta_0$ with $\dot{r} = 0$, one inside the region bounded by $W^s_{\theta_0,n-1}(\gamma_1)$ or $W^s_{\theta_0,n-1}(\gamma_2)$ and the other one outside that region. We found that one point is stable and the other is unstable in the sense of the algorithmic definition of the WSB.

5. Conclusions. In this paper we provided a geometric argument, based on the separatrix property of the invariant manifolds of the Lyapunov orbits, for the fact that, for some range of energies, the points on the stable manifold of the Lyapunov orbits about L_1 and L_2 are points in the WSB, provided that these points satisfy the zero radial velocity condition and the negative Kepler energy condition relative to the small primary. We supported our geometric argument with numerical experiments. This geometric argument justifies the numerical findings in [18]. The results in this paper, corroborated with those in [18], establish that the WSB method for the design of fuel efficient spacecraft trajectories substantially overlaps with the invariant manifold method.

A consequence of our findings is that the algorithmic definition of the WSB provides a method of finding trajectories on the stable manifold of a Lyapunov orbit which does not require the a priori knowledge of the Lyapunov orbit. In particular, one can obtain symmetric homoclinic orbits. This type of approach contrasts with the traditional method for computing the stable manifold of a Lyapunov orbit, which first computes the Lyapunov orbit and then integrates nearby initial conditions in the direction of the stable eigenvectors. It is well known that long-term integration of the invariant manifolds is prone to large numerical errors. It seems possible that the algorithmic definition of the WSB can be used as a method of verification and correction for long-term integration of the invariant manifolds.

The existence of homoclinic points inside the WSB is consistent with the results shown analytically in [3] in the case of near-parabolic motion. However, our numerical experiments indicate that the WSB contains symmetric homoclinic points for the whole range of Jacobi constants for which the WSB is defined.

Weak stability boundaries exist even in models where the hyperbolic invariant manifolds are no longer well defined. It seems possible that the WSB may turn out to provide a good substitute for the hyperbolic invariant manifolds in such models. We believe that this idea could be exploited in space mission design and should be explored further.

REFERENCES

[1] E. M. Alessi, G. Gómez, and J. J. Masdemont, *Leaving the Moon by the means of the invariant manifolds of libration point orbits*, Commun. Nonlinear Sci. Numer. Simul., 14 (2009), pp. 4153–4167.

[2] E. Belbruno, *Lunar capture orbits, A method for constructing Earth-Moon trajectories and the lunar GAS mission*, in Proceedings of the AIAA/DGLR/JSASS International Propl. Conf., Colorado Springs, CO, 1987, AIAA paper 87-1054.

[3] E. Belbruno, *Capture Dynamics and Chaotic Motions in Celestial Mechanics*, Princeton University Press, Princeton, NJ, 2004.

[4] E. Belbruno, *Fly Me to the Moon: An Insiders Guide to the New Science of Space Travel*, Princeton University Press, Princeton, NJ, 2007.

[5] E. Belbruno and B. Marsden, *Resonance hopping in comets*, Astronom. J., 113 (1997), pp. 1433–1444.

[6] E. Belbruno and J. Miller, *Sun-perturbed Earth-to-Moon transfers with ballistic capture*, J. Guidance Control Dynam., 16 (1993), pp. 770–775.

[7] E. Belbruno and J. Miller, *A Ballistic Lunar Capture Trajectory for the Japanese Spacecraft Hiten*, technical report, IOM 312/90.4–1371-EAB, Jet Propulsion Laboratory, Pasadena, CA, 1990.

[8] R. A. Broucke, *Periodic Orbits in the Restricted Three-Body Problem with. Earth-Moon Masses*, NASA-JPL Technical Report 32-1168, Jet Propulsion Laboratory, Pasadena, CA, 1968.

[9] K. Burns and M. Gidea, *Differential Geometry and Topology: With a View to Dynamical Systems*, Chapman & Hall/CRC Press, Boca Raton, FL, 2005.

[10] E. Canalias and J. J. Masdemont, *Homoclinic and heteroclinic transfer trajectories between planar Lyapunov orbits in the Sun-Earth and Earth-Moon systems*, Discrete Contin. Dyn. Syst., 14 (2006), pp. 261–279.

[11] A. Celletti and L. Chierchia, *KAM stability and celestial mechanics*, Mem. Amer. Math. Soc., 187 (2007), no. 878.

[12] C. Circi, F. Graziani, M. Porfilio, and P. Teofilatto, *Weak stability boundary lunar transfers from Soyouz and Rockot planar launches*, in Proceedings of the 22nd International Symposium on Space Technology and Science, Morioka, Japan, 2000, pp. 1555–1563.

[13] C. Circi and P. Teofilato, *On the dynamics of weak stability boundary lunar transfers*, Celestial Mech. Dyn. Astron., 79 (2001), pp. 41–72.

[14] C. Circi and P. Teofilato, *Weak stability boundary trajectories for the deployment of lunar spacecraft constellations*, Celestial Mech. Dyn. Astron., 95 (2006), pp. 371–390.

[15] C. C. Conley, *Low energy transit orbits in the restricted three-body problem*, SIAM J. Appl. Math., 16 (1968), pp. 732–746.

[16] E. J. Doedel, V. A. Romanov, R. C. Paffenroth, H. B. Keller, D. J. Dichmann, J. Galán-Vioque, and A. Vanderbauwhede, *Elemental periodic orbits associated with the libration points in the circular restricted 3-body problem*, Internat. J. Bifur. Chaos Appl. Sci. Engrg., 17 (2007), pp. 2625–2677.

[17] R. W. Easton and R. McGehee, *Homoclinic phenomena for orbits doubly asymptotic to an invariant three-sphere*, Indiana Univ. Math. J., 28 (1979), pp. 211–240.

[18] F. García and G. Gómez, *A note on weak stability boundaries*, Celestial Mech. Dyn. Astron., 97 (2007), pp. 87–100.

[19] E. S. Gawlik, P. C. Du Toit, S. Campagnola, and J. E. Marsden, *Lagrangian coherent structures in the planar elliptic restricted three-body problem*, Celestial Mech. Dyn. Astron., 103 (2009), pp. 227–249.

[20] M. Gidea and J. J. Masdemont, *Geometry of homoclinic connections in a planar circular restricted three-body problem*, Internat. J. Bifur. Chaos Appl. Sci. Engrg., 17 (2007), pp. 1151–1169.

[21] G. Gomez, J. Llibre, R. Martinez, and C. Simo, *Dynamics and Mission Design near Libration*

Points, Volume I. *Fundamentals: The Case of Collinear Libration Points*, World Sci. Monogr. Ser. Math., World Scientific, River Edge, NJ, 2001.

[22] G. GOMEZ, J. LLIBRE, R. MARTINEZ, AND C. SIMO, *Dynamics and Mission Design near Libration Points, Volume* II. *Fundamentals: The Case of Triangular Libration Points*, World Sci. Monogr. Ser. Math., World Scientific, River Edge, NJ, 2001.

[23] G. GÓMEZ, Á. JORBA, C. SIMÓ, AND J. J. MASDEMONT, *Dynamics and Mission Design near Libration Points, Volume* III. *Advanced Methods for Collinear Points*, World Sci. Monogr. Ser. Math., World Scientific, River Edge, NJ, 2001.

[24] G. GÓMEZ, Á. JORBA, C. SIMÓ, AND J. J. MASDEMONT, *Dynamics and Mission Design near Libration Points, Volume* IV. *Advanced Methods for Triangular Points*, World Sci. Monogr. Ser. Math., World Scientific, River Edge, NJ, 2001.

[25] R. JEHN, S. CAMPAGNOLA, D. GARCÍA, AND S. KEMBLE, *Low-thrust approach and gravitational capture at Mercury*, in Proceedings of the 18th International Symposium on Space Flight Dynamics, Munich, 2004, ESA Publications, pp. 487–492.

[26] S. JERG, O. JUNGE, AND S. ROSS, *Optimal capture trajectories using multiple gravity assist*, Commun. Nonlinear Sci. Numer. Simul., 14 (2009), pp. 4168–4175.

[27] W. S. KOON, M. W. LO, J. E. MARSDEN, AND S. D. ROSS, *Heteroclinic connections between periodic orbits and resonance transitions in celestial mechanics*, Chaos, 10 (2000), pp. 427–469.

[28] W. S. KOON, M. W. LO, J. E. MARSDEN, AND S. D. ROSS, *Low energy transfer to the Moon*, Celestial Mech. Dyn. Astron., 81 (2001), pp. 63–73.

[29] M. KUMMER, *On the stability of Hill's solutions of the plane restricted three-body problem*, Amer. J. Math., 101 (1979), pp. 1333–1354.

[30] J. LLIBRE, R. MARTÍNEZ, AND C. SIMÓ, *Transversality of the invariant manifolds associated to the Lyapunov family of periodic orbits near L_2 in the restricted three-body problem*, J. Differential Equations, 58 (1985), pp. 104–156.

[31] M. LO AND S. ROSS, *SURFing the Solar System: Invariant Manifolds and the Dynamics of the Solar System*, JPL technical report IOM 312/97, 2-4, Jet Propulsion Laboratory, Pasadena, CA, 1997.

[32] M. W. LO, R. L. ANDERSON, G. WHIFFEN, AND L. ROMANS, *The role of invariant manifolds in low thrust trajectory design*, in Advances in the Astronautical Sciences 119, AAS, Springfield, VA, 2004, pp. 2971–2990.

[33] E. E. N. MACAU, *Book review: Capture Dynamics and Chaotic Motions in Celestial Mechanics by Edward Belbruno, Princeton University Press, Princeton/Oxford,* 2004, Celestial Mech. Dyn. Astron., 91 (2005), pp. 407–408.

[34] R. P. MCGEHEE, *Some Homoclinic Orbits for the Restricted Three-Body Problem*, Ph.D. thesis, Department of Mathematics, University of Wisconsin, Madison, WI, 1969.

[35] C. F. DE MELO AND O. C. WINTER, *Alternative paths to Earth-Moon transfer*, Math. Probl. Engrg., 2006 (2006), pp. 1–20.

[36] J. MOSER, *Stable and Random Motions in Dynamical Systems*, Princeton University Press, Princeton, NJ, 1973.

[37] J. POSCHEL, *On Nekhoroshev's estimate for quasi-convex Hamiltonians*, Math. Z., 5 (1993), pp. 187–216.

[38] D. ROMAGNOLI AND C. CIRCI, *Earth-Moon weak stability boundaries in the restricted three and four body problem*, Celestial Mech. Dyn. Astron., 103 (2009), pp. 79–103.

[39] S. ROSS, *Fly Me to the Moon—A book review*, Notices Amer. Math. Soc., 55 (2008), pp. 478–480.

[40] J. SCHOENMAEKERS, D. HORAS, AND J. A. PULIDO, *SMART*-1: *With solar electric propulsion to the Moon*, in Proceedings of the 16th International Symposium on Space Flight Dynamics, Pasadena, CA, 2001, pp. 114–130.

[41] C. L. SIEGEL AND J. MOSER, *Lectures on Celestial Mechanics*, Grundlehren Math. Wiss. 187, Springer-Verlag, Berlin, Heidelberg, 1971.

[42] C. SIMÓ AND T. STUCHI, *Central stable/unstable manifolds and the destruction of KAM tori in the planar Hill problem*, Phys. D, 140 (2000), pp. 1–32.

[43] V. SZEBEHELY, *Theory of Orbits*, Academic Press, Orlando, FL, 1967.

[44] F. TOPPUTO AND E. BELBRUNO, *Computation of the weak stability boundaries: Sun-Jupiter system*, Celestial Mech. Dyn. Astron., 105 (2009), pp. 3–17.

[45] K. YAGASAKI, *Sun-perturbed Earth-to-Moon transfers with low energy and moderate flight time*, Celestial Mech. Dyn. Astron., 90 (2004), pp. 197–212.